Faculty of Mathematics and Physics
Charles University in Prague

NUMERICAL SIMULATIONS OF THE MAGNETOHYDRODYNAMIC SYSTEM

Jakub Velímský

Praha 1998

Faculty of Mathematics and Physics
Charles University in Prague

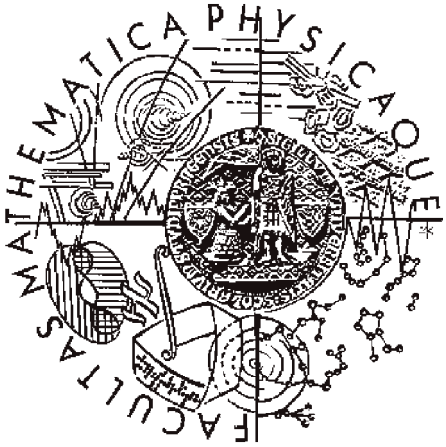

NUMERICAL SIMULATIONS OF THE MAGNETOHYDRODYNAMIC SYSTEM

Diploma Thesis

Author: Jakub Velímský

Supervisor: doc. RNDr. Ctirad Matyska, DrSc.

Department of Geophysics
V Holešovičkách 2
180 00 Praha 8
Czech Republic

Praha 1998

Prohlašuji, že jsem diplomovou práci vypracoval samostatně a že jsem použil pouze uvedenou literaturu. Souhlasím ze zapůjčováním diplomové práce.

Contents

1 Introduction **5**
1.1 Generation of the Geomagnetic Field 5
1.2 Description of the Model 5

2 Conductive Fluid in a Three-dimensional Box **9**
2.1 Basic Equations 9
2.1.1 Hydrodynamic Equations 9
2.1.2 Magnetic Equations 12
2.2 Computational Domain 13
2.3 Boundary Conditions 14
2.4 Dimensionless Equations 15
2.5 Vorticity 17

3 Numerical Methods **19**
3.1 Spatial Derivatives Approximation 19
3.1.1 Finite Difference Method 19
3.1.2 Discrete Boundary Conditions 20
3.2 Discrete Fourier Transform 23
3.3 Time Evolution 24

4 Results **27**
4.1 Parameters of the Models 27
4.2 Integral Quantities 29
4.3 Case I 31
4.4 Case II 39
4.5 Case III 45
4.6 Numerical Stability 53

5 Conclusions **55**

References **57**

Acknowledgements **59**

Chapter 1

Introduction

1.1 Generation of the Geomagnetic Field

The question of the origin of geomagnetic field attracted the attention of scientists for centuries. The first theory of the geomagnetic field source was Gilbert's idea of a permanent magnet within the Earth. It had to be abandoned, because it did not agree with the observation of the secular variation of the field. Neither the theory of geomagnetic field generated by rotation, nor the flow of free electrons in the Earth were able to explain properties of the field.

Better understanding of the Earth's interior, especially the discovery of the liquid core in 1906, together with the advance in fluid dynamics and electrodynamics, brought into being the dynamo theory of geomagnetism. Electrically conductive fluid is forced to circulate in the Earth's outer core by the combined effect of the Lorentz, Coriolis, thermal and compositional buoyancy forces. Due to the presence of magnetic field, the motion of the fluid generates electric currents, which are responsible for the generation of magnetic field according to the Ampère law. As we will show in *Chapter 2*, such a behaviour is described by a set of complicated, nonlinear, evolutionary equations, even if we accept some important simplifications.

Three-dimensional, self-consistent and time-dependent solutions of this system on a spherical shell [7, 8] require incredible computational power, which was not available at all until the recent days. Therefore many simplifications and approximations are used to study this phenomenon. The kinematic dynamo theory [1, 13], which is interested only in the evolution of magnetic field and considers the motion of the fluid to be known, is an example of such a simplification. We use a different approach, as described in the next section.

1.2 Description of the Model

We will study the time evolution of self-consistent magnetohydrodynamic equations in a three-dimensional rectangular box, which is considered to be a part of the spherical shell (see Fig. 1.1), situated below the North

Pole. Although from the hydrodynamic point of view it would be possible to position the rectangular area in the core by different ways [11], the choice of boundary conditions suitable for magnetic induction in such a domain is questionable. Using the rectangular box is an important simplification, because it introduces new boundaries — sidewalls, that do not exist in the real core. Also the centre of the Earth is stretched into a new boundary plane. On the other hand, limiting ourselves to a smaller computational domain increases our spatial resolution. It also allows us to perform all the computations in Cartesian coordinates.

The other assumptions, that we suppose, are more acceptable. We consider the fluid in the outer core to be Newtonian. Because the viscosity in the core is poorly determined and, moreover, the estimated values are far behind our computational reach, introducing a more complicated rheological model would be of no use. For similar reasons, we use the Ohm law to describe the electrical behaviour of the fluid and consider the outer and inner core to be electromagnetically homogeneous and isotropic.

It is supposed, that the Earth's outer core consists mainly of iron, with addition of light elements. Iron freezes on the inner core boundary (ICB), resulting in the growth of the inner core, while the release of light elements and heat at this boundary drives the convection. In our simulation, we do not take into account the compositional buoyancy, i.e. we consider the fluid to be homogeneous. Although the compositional driving may be larger than the thermal driving, they are both governed by similar equations and their influence on the convection is also similar [8]. We will use the Boussinesq approximation of the state equation, which neglects the pressure dependency

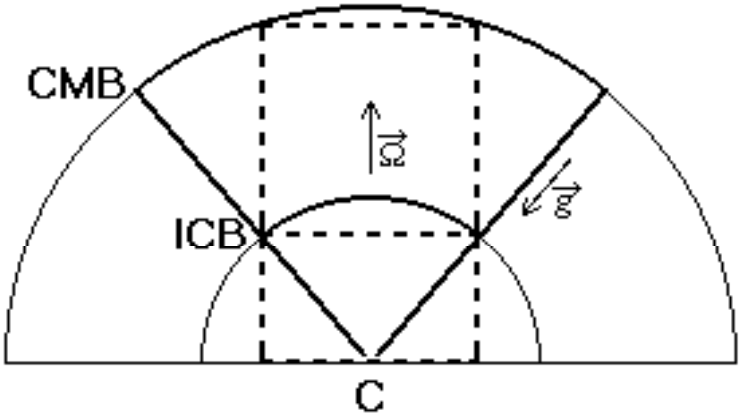

Figure 1.1: Position of the computational domain in the Earth's core.

of density and allows to take into account only the temperature dependency of density in the gravitational force. The thermodynamic parameters describing the fluid are constant both in space and time.

The radial gravitational field is replaced by a homogeneous one, acting downward in the z-axis direction. Our model includes the Coriolis force with rotation axis parallel to z-axis, the inertial force and the Lorentz force.

Also the boundary conditions of our model are simpler than those in the Earth. Instead of rigid boundary conditions for the velocity at the core–mantle boundary (CMB) and ICB, we use impermeable, free-slip boundary conditions, which result in similar physical behaviour of the boundary, while being more suitable for the vorticity formulation of the problem, as will be described in *Chapter 2*. We also prescribe the temperature values at the CMB and ICB, allowing the heat flux through them. As for the magnetic induction, we solve the diffusion equation in the inner core box, allowing only the z-component to be non-zero at its bottom plane. We consider the Earth's mantle to be an insulator, because its conductivity is at least two orders smaller than the conductivity of the core. In other words, we do not allow the electromagnetic coupling at the CMB. The boundary conditions at the sidewalls assure that no mass, no heat flux and no magnetic field leaves the box.

Chapter 2

Conductive Fluid in a Three-dimensional Box

2.1 Basic Equations

2.1.1 Hydrodynamic Equations

The Earth's outer core can be considered as a conductive fluid continuum. Such a material obeys basic laws of conservation of four quantities: mass, momentum, moment of momentum and energy. The differential form of these laws written in Euler's coordinate system, i.e. with respect to the deformed state, is

$$\frac{\partial \rho}{\partial t} + \nabla \cdot (\rho \vec{v}) = 0, \tag{2.1}$$

$$\rho \frac{D\vec{v}}{Dt} = \nabla \cdot \overleftrightarrow{\tau} + \vec{f}, \tag{2.2}$$

$$\overleftrightarrow{\tau} = \overleftrightarrow{\tau}^T, \tag{2.3}$$

$$\rho T \frac{Ds}{Dt} = \nabla \cdot (k \nabla T) + \overleftrightarrow{\sigma} : \nabla \vec{v} + \frac{\lambda}{\mu_0} (\nabla \times \vec{B})^2 + Q, \tag{2.4}$$

where the meaning of all symbols is explained in Tab. 2.1. If we consider dominantly hydrostatic pressure, the equation (2.4) can be written as follows,

$$\rho C_p \frac{\partial T}{\partial t} = \nabla \cdot (k \nabla T) - \rho C_p \vec{v} \cdot \nabla T - \alpha T \rho g \vec{v} \cdot \vec{e}_z + \overleftrightarrow{\sigma} : \nabla \vec{v} + \frac{\lambda}{\mu_0} (\nabla \times \vec{B})^2 + Q. \tag{2.5}$$

In our work we will consider three volume forces acting on the fluid: the Coriolis force, the Lorentz force and the gravitational force (caused by a homogeneous gravity field), i.e.,

$$\vec{f} = -2\vec{\Omega} \times \vec{v} + \frac{1}{\mu_0} (\nabla \times \vec{B}) \times \vec{B} + \rho \vec{g}. \tag{2.6}$$

Two more equations are needed to fully describe the fluid: a rheological relationship and an equation of state. We will use the Newtonian rheology given by the equations

$$\overleftrightarrow{\tau} = -p \overleftrightarrow{\mathrm{I}} + \overleftrightarrow{\sigma}. \tag{2.7}$$

$$\overleftrightarrow{\sigma} = \eta[\nabla\vec{v} + (\nabla\vec{v})^T - \frac{2}{3}\overleftrightarrow{\mathrm{I}}\nabla\cdot\vec{v}]. \tag{2.8}$$

Note, that this relation satisfies the law of conservation of moment of momentum (2.3).

The Boussinesq approximation of the state equation, as was described in *Chapter 1*, leads to the substitution of ρ in the third term of equation (2.6) by

$$\rho = \rho_0[1 - \alpha(T - T_0)]. \tag{2.9}$$

In all other terms we will consider

$$\rho = \rho_0. \tag{2.10}$$

All physical parameters describing the fluid, e.g. λ, η, k, α, C_p, ρ_0 (see Tab. 2.1), are constant.

Taking into account these assumptions, (2.1) implies the incompressibility of the fluid

$$\nabla\cdot\vec{v} = 0 \tag{2.11}$$

and thus the non-reversible part of the stress tensor in the rheological relation (2.8) simplifies into

$$\overleftrightarrow{\sigma} = \eta[\nabla\vec{v} - (\nabla\vec{v})^T]. \tag{2.12}$$

Substituting (2.6), the rheology (2.7), (2.12) and the density (2.9), (2.10) into the momentum equation (2.2) yields

$$\begin{aligned}\rho_0(\frac{\partial\vec{v}}{\partial t} + \vec{v}\cdot\nabla\vec{v}) &= \eta\Delta\vec{v} - \nabla p - 2\rho_0\Omega\times\vec{v} + \frac{1}{\mu_0}(\nabla\times\vec{B})\times\vec{B} + \\ &\quad +\rho_0\vec{g} - \rho_0\alpha(T - T_0)\vec{g}.\end{aligned} \tag{2.13}$$

The gradient of the hydrostatic pressure is given by relation

$$\nabla p_0 = \rho_0\vec{g}. \tag{2.14}$$

We will introduce the pressure Π as a deviation from the reference hydrostatic pressure,

$$\Pi = p - p_0. \tag{2.15}$$

Now we can finally write

$$\rho_0(\frac{\partial\vec{v}}{\partial t} + \vec{v}\cdot\nabla\vec{v}) = \eta\Delta\vec{v} - \nabla\Pi - 2\rho_0\Omega\times\vec{v} + \frac{1}{\mu_0}(\nabla\times\vec{B})\times\vec{B} - \rho_0\alpha(T - T_0)\vec{g}. \tag{2.16}$$

By applying the Boussinesq approximation on the law of conservation of energy (2.5) we get

$$\rho_0 C_p\frac{\partial T}{\partial t} = k\Delta T + \overleftrightarrow{\sigma} : \nabla\vec{v} - \rho_0 C_p\vec{v}\cdot\nabla T - \alpha T\rho_0 g\vec{v}\cdot\vec{e}_z + \frac{\lambda}{\mu_0}(\nabla\times\vec{B})^2 + Q. \tag{2.17}$$

Symbol	Meaning	SI Unit
t	time	s
d	vertical size of the outer core box	m
d_i	vertical size of the inner core box	m
a_x, a_y	horizontal sizes of the box relative to d	1
$\vec{e}_x$, $\vec{e}_y$, $\vec{e}_z$	unit base vectors (orthogonal)	1
$\vec{n}$	unit vector perpendicular to the boundary	1
$\vec{v}$	velocity	$\mathrm{m\,s^{-1}}$
T	temperature	K
T_0	temperature at the CMB	K
δT	temperature drop between ICB and CMB	K
ρ	density	$\mathrm{kg\,m^{-3}}$
ρ_0	reference density at T_0	$\mathrm{kg\,m^{-3}}$
$\overleftrightarrow{\tau}$	Cauchy's stress tensor	Pa
$\overleftrightarrow{\sigma}$	non reversible part of Cauchy's tensor	Pa
$\overleftrightarrow{\mathrm{I}}$	identical tensor	1
$\vec{f}$	total volume force acting on the fluid	$\mathrm{N\,m^{-3}}$
$\vec{\Omega}$	Earth's rotation	$\mathrm{rad\,s^{-1}}$
$\vec{k}$	unit vector of Earth's rotation	1
p	pressure	Pa
p_o	hydrostatic pressure	Pa
Π	deviation of pressure from hydrostatic state	Pa
η	dynamic viscosity	Pa s
ν	kinematic viscosity	$\mathrm{m^2\,s^{-1}}$
$\vec{g}$	gravitational acceleration	$\mathrm{m\,s^{-2}}$
s	density of entropy	$\mathrm{m^2\,s^{-2}\,K^{-1}}$
k	thermal conductivity	$\mathrm{kg\,m\,s^{-3}\,K^{-1}}$
κ	thermal diffusivity	$\mathrm{m^2\,s^{-1}}$
α	thermal expansivity	$\mathrm{K^{-1}}$
Q	internal heating rate	$\mathrm{kg\,m^{-1}\,s^{-3}}$
C_p	specific heat at a constant pressure	$\mathrm{m^2\,s^{-2}\,K^{-1}}$
$\vec{B}$	magnetic induction	T
$\vec{H}$	intensity of the magnetic field	$\mathrm{A\,m^{-1}}$
$\vec{E}$	intensity of the electric field	$\mathrm{V\,m^{-1}}$
$\vec{D}$	electric induction	$\mathrm{C\,m^{-2}}$
$\vec{j}$	density of electric current	$\mathrm{A\,m^{-1}}$
ρ_e	density of electric charge	$\mathrm{C\,m^{-3}}$
ϵ	permitivity	$\mathrm{F\,m^{-1}}$
μ_0	permeability	$\mathrm{H\,m^{-1}}$
σ	electric conductivity	$\mathrm{\Omega^{-1}\,m^{-1}}$
λ	magnetic diffusivity	$\mathrm{m^2\,s^{-1}}$

Table 2.1: List of symbols.

2.1.2 Magnetic Equations

The electromagnetic field is governed by four Maxwell's equations which can be written as

$$\nabla \cdot \vec{B} = 0, \tag{2.18}$$

$$\nabla \cdot \vec{D} = \rho_e, \tag{2.19}$$

$$\nabla \times \vec{H} = \vec{\jmath} + \frac{\partial \vec{D}}{\partial t}, \tag{2.20}$$

$$\nabla \times \vec{E} = -\frac{\partial \vec{B}}{\partial t}, \tag{2.21}$$

Of course, relations describing the electromagnetic properties of the fluid must be added. We consider the fluid to be electromagnetically homogeneous, isotropic and linear, i.e. to obey the Ohm law:

$$\vec{D} = \epsilon \vec{E}, \qquad \epsilon = const, \tag{2.22}$$

$$\vec{B} = \mu_0 \vec{H}, \qquad \mu_0 = const, \tag{2.23}$$

$$\vec{\jmath} = \sigma(\vec{E} + \vec{v} \times \vec{B}), \qquad \sigma = const, \tag{2.24}$$

Let us assume, that the electric induction changes slowly and that the second term in equation (2.20) can be neglected

$$\frac{\partial \vec{D}}{\partial t} \ll \vec{\jmath}. \tag{2.25}$$

This assumption is well satisfied in the Earth's inner and outer core, with characteristic times of order higher than 10^2 yr, and EM waves periods of order 10^{-2} s only. Then applying the operator $\nabla\times$ to the equation (2.20) and substitution from (2.18), (2.21), (2.23) and (2.24) to (1.20) yields:

$$\frac{\partial \vec{B}}{\partial t} = \lambda \Delta \vec{B} + \nabla \times (\vec{v} \times \vec{B}), \tag{2.26}$$

where

$$\lambda = \frac{1}{\mu_0 \sigma}. \tag{2.27}$$

Equations (2.26) and (2.18) describe the magnetic field in the fluid. Let us apply the differential operator $\nabla\cdot$ to (2.26). We get

$$\frac{\partial (\nabla \cdot \vec{B})}{\partial t} = \lambda \Delta (\nabla \cdot \vec{B}). \tag{2.28}$$

Thus, if we choose at the time t_0 such an initial field $\vec{B}(x, y, z, t_0)$, that

$$\nabla \cdot \vec{B}(x, y, z, t_0) = 0 \tag{2.29}$$

then the equation (2.18) should be satisfied as well for $\vec{B}(x, y, z, t), t > t_0$ (assuming, that we can compute the field $\vec{B}$ with no errors). So we can omit it and use only the equation (2.26) for computing the magnetic field.

In the solid inner core the equation (2.26) simplifies:

$$\frac{\partial \vec{B}}{\partial t} = \lambda \Delta \vec{B}. \tag{2.30}$$

2.2 Computational Domain

As we have already mentioned in the introduction, we will solve the system of equations (2.11), (2.16), (2.17) and (2.26) in a three-dimensional rectangular box with dimensions $(a_x\, d, a_y\, d, d)$ (see Fig. 2.1). The bottom of the box corresponds to the inner core boundary (ICB) and its top reaches the core-mantle boundary (CMB). We will also compute the magnetic induction, according to (2.30), in the inner core, i.e. in the box with dimensions $(a_x\, d, a_y\, d, d_i)$. The bottom of this box is considered to be "the centre of the Earth".

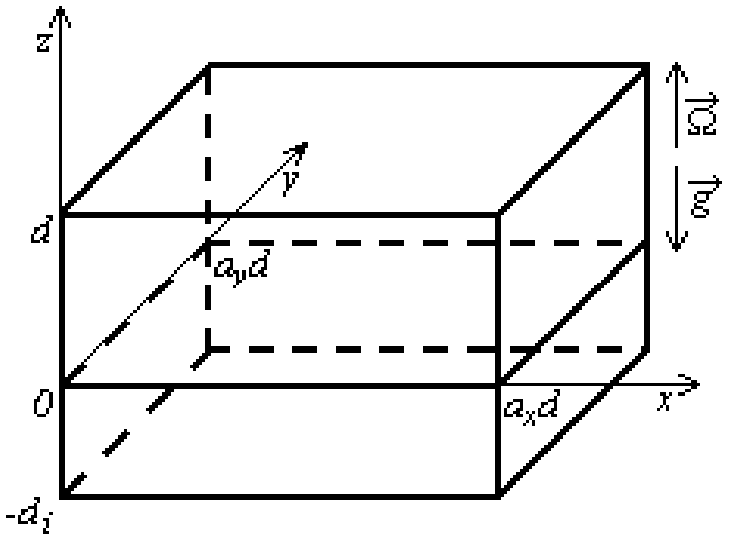

Figure 2.1: The computational domain.

2.3 Boundary Conditions

We will use impermeable, free-slip boundary conditions at the boundaries of the box:

$$(\vec{v} \cdot \vec{n})_{sidewalls,CMB,ICB} = 0, \tag{2.31}$$

$$[\overleftrightarrow{\tau} \cdot \vec{n} - (\vec{n} \cdot \overleftrightarrow{\tau} \cdot \vec{n})\vec{n}]_{sidewalls,CMB,ICB} = 0. \tag{2.32}$$

Substituting $\overleftrightarrow{\tau}$ from (2.7) and (2.12) yields

$$(v_n = \frac{\partial v_t}{\partial n} = \frac{\partial v_s}{\partial n})_{sidewalls,CMB,ICB} = 0. \tag{2.33}$$

Subscript n corresponds to the normal component of the vector, subscripts t and s describe the tangential components of the vector.

As for the temperature, we prescribe its values at the top and the bottom:

$$(T)_{CMB} = T_0, \tag{2.34}$$

$$(T)_{ICB} = T_0 + \delta T \tag{2.35}$$

and we require no heat flux through the sidewalls,

$$(\frac{\partial T}{\partial n})_{sidewalls} = 0. \tag{2.36}$$

The boundary conditions for magnetic induction $\vec{B}$ are more complicated. We will require, that no magnetic field leaves the box through the sidewalls. This condition will be applied to both the outer and inner core boxes, i.e.

$$(B_n = \frac{\partial B_t}{\partial n} = \frac{\partial B_s}{\partial n})_{sidewalls} = 0. \tag{2.37}$$

There is no boundary condition for $\vec{B}$ at the ICB, because the field is computed also in the lower box. At the bottom of the lower box, in the centre of the Earth, we require the tangential components of $\vec{B}$ to vanish and the normal component to be continuous, i.e.

$$(B_t = B_s = \frac{\partial B_n}{\partial n})_C = 0. \tag{2.38}$$

At the CMB, the situation is different. We will consider the Earth's mantle to be an electric insulator. It means, that the magnetic field in the mantle will be governed by equation (2.26) for $\lambda \to \infty$, i.e.

$$\Delta \vec{B} = 0. \tag{2.39}$$

Now, let us expand $\vec{B}$ into the Fourier series with respect to x and y:

$$\vec{B}(x,y,z) = \sum_{p,q=0}^{\infty} \hat{\vec{B}}_{pq}(z) e^{[2\pi i(\frac{p\,x}{a_x\,d} + \frac{q\,y}{a_y\,d})]}. \tag{2.40}$$

Equation (2.39) then implies

$$\frac{d^2\hat{\vec{B}}_{pq}(z)}{d^2 z} - 4\pi^2[(\frac{p}{a_x\,d})^2 + (\frac{q}{a_y\,d})^2]\hat{\vec{B}}_{pq}(z) = 0, \qquad \forall\, p,q. \tag{2.41}$$

The solution of (2.41), that does not diverge for $z \to \infty$, has the following form

$$\hat{\vec{B}}_{pq}(z) = \hat{\vec{B}}_{pq}(d) e^{[-2\pi\sqrt{(\frac{p}{a_x\,d})^2 + (\frac{q}{a_y\,d})^2}\,(z-d)]}. \tag{2.42}$$

We can see, that the terms of two-dimensional Fourier series of $\vec{B}$ exponentially decay in the mantle.

2.4 Dimensionless Equations

It is useful to rewrite the system of equations (2.11), (2.16), (2.17) and (2.26) by means of dimensionless variables. It allows us to minimize the set of parameters needed to describe the fluid. We will use the following scaling equations (new dimensionless quantities are primed, note that also the operator ∇ must be rescaled)

$$\vec{x} = d\vec{x}', \tag{2.43}$$

$$\nabla = \frac{1}{d}\nabla', \tag{2.44}$$

$$t = \frac{d^2}{\lambda}t', \tag{2.45}$$

$$\vec{v} = \frac{\lambda}{d}\vec{v}', \tag{2.46}$$

$$\Pi = \frac{\eta\lambda}{d^2}\Pi', \tag{2.47}$$

$$T = T_0 + \delta T\, T', \tag{2.48}$$

$$\vec{B} = \sqrt{2\rho_0\Omega\mu_0\lambda}\vec{B}', \tag{2.49}$$

$$\overleftrightarrow{\sigma} = \frac{\eta\lambda}{d^2}\overleftrightarrow{\sigma}', \tag{2.50}$$

$$Q = \frac{\rho_0 C_p \lambda \delta T}{d^2} Q'. \tag{2.51}$$

We also introduce new quantities - thermal diffusivity and kinematic viscosity by the relations

$$\kappa = \frac{k}{\rho_0 C_p}, \tag{2.52}$$

$$\nu = \frac{\eta}{\rho_0}. \tag{2.53}$$

With these new variables we can write the system of magnetohydrodynamic equations as follows (from now, primes will be omitted, because we will use only dimensionless variables)

$$\nabla \cdot \vec{v} = 0, \tag{2.54}$$

$$\begin{aligned} \frac{\partial \vec{v}}{\partial t} &= \frac{\nu}{\lambda}\Delta\vec{v} - \vec{v}\cdot\nabla\vec{v} - \frac{\nu}{\lambda}\nabla\Pi + \frac{\alpha g d^3 \delta T}{\lambda^2} T\vec{e}_z - \\ &\quad - \frac{2\Omega d^2}{\lambda}\vec{k}\times\vec{v} + \frac{2\Omega d^2}{\lambda}(\nabla\times\vec{B})\times\vec{B}, \end{aligned} \tag{2.55}$$

$$\begin{aligned} \frac{\partial T}{\partial t} &= \frac{k}{\rho_0 C_p \lambda}\Delta T - \vec{v}\cdot\nabla T + \frac{\eta\lambda}{\rho_0 C_p d^2 \delta T}\overleftrightarrow{\sigma} : \nabla\vec{v} - \frac{\alpha g d}{C_p}(T + \frac{T_0}{\delta T})\vec{v}\cdot\vec{e}_z + \\ &\quad + \frac{2\Omega\lambda}{C_p\delta T}(\nabla\times\vec{B})^2 + Q, \end{aligned} \tag{2.56}$$

$$\frac{\partial \vec{B}}{\partial t} = \Delta\vec{B} + \nabla\times(\vec{v}\times\vec{B}). \tag{2.57}$$

The equation (2.12) in dimensionless variables also changes,

$$\overleftrightarrow{\sigma} = \nabla\vec{v} + (\nabla\vec{v})^T. \tag{2.58}$$

Now we can introduce five parameters. They are called Prandtl, Prandtl magnetic, Rayleigh, Taylor and dissipative numbers and are defined in the following way:

$$Pr = \frac{\nu}{\kappa}, \tag{2.59}$$

$$Pm = \frac{\nu}{\lambda}, \tag{2.60}$$

$$Ra = \frac{\alpha g d^3 \delta T}{\kappa\nu}, \tag{2.61}$$

$$Ta = \frac{4d^4\Omega^2}{\nu^2}, \tag{2.62}$$

$$Dn = \frac{\alpha g d}{C_p}. \tag{2.63}$$

The five parameters mentioned above, the ratio $\frac{T_0}{\delta T}$ and the internal heating rate Q characterize the magnetohydrodynamic system.

Using these numbers we can finally write:

$$\nabla \cdot \vec{v} = 0, \tag{2.64}$$

$$\begin{aligned} \frac{\partial \vec{v}}{\partial t} &= Pm\,\Delta\vec{v} - \vec{v}\cdot\nabla\vec{v} - Pm\,\nabla\Pi + \frac{(Pm)^2\,Ra}{Pr}T\vec{e}_z - \\ &\quad -Pm\,\sqrt{Ta}\,\vec{k}\times\vec{v} + Pm\,\sqrt{Ta}\,(\nabla\times\vec{B})\times\vec{B}, \end{aligned} \tag{2.65}$$

$$\begin{aligned} \frac{\partial T}{\partial t} &= \frac{Pm}{Pr}\Delta T - \vec{v}\cdot\nabla T + \frac{Dn\,Pr}{Ra\,Pm}\overleftrightarrow{\sigma} : \nabla\vec{v} + \frac{Dn\,Pr\,\sqrt{Ta}}{Ra\,Pm}(\nabla\times\vec{B})^2 - \\ &\quad -Dn\,(T + \frac{T_0}{\delta T})\vec{v}\cdot\vec{e}_z + Q, \end{aligned} \tag{2.66}$$

$$\frac{\partial \vec{B}}{\partial t} = \Delta\vec{B} + \nabla\times(\vec{v}\times\vec{B}). \tag{2.67}$$

The boundary conditions for velocity $\vec{v}$ and magnetic induction $\vec{B}$, as described in (2.33), (2.37), (2.38) and (2.42) remain unchanged for dimensionless quantities. Also the condition (2.36) for temperature at the sidewalls does not change. However, the dimensionless temperature at the top and the bottom of the box is

$$(T)_{CMB} = 0, \tag{2.68}$$

$$(T)_{ICB} = 1. \tag{2.69}$$

2.5 Vorticity

Equations (2.64) and (2.65) represent four scalar equations for computing three components of velocity $\vec{v}$ and pressure Π. Let us define vorticity of the velocity field as

$$\vec{\omega} = \nabla\times\vec{v}. \tag{2.70}$$

Then applying $\nabla\times$ to (2.65) yields

$$\begin{aligned}\frac{\partial\vec{\omega}}{\partial t} &= Pm\,\Delta\vec{\omega}+\vec{\omega}\cdot\nabla\vec{v}-\vec{v}\cdot\nabla\vec{\omega}+\\ &\quad+\frac{(Pm)^2\,Ra}{Pr}\nabla\times(T\vec{e}_z)+Pm\sqrt{Ta}\,\vec{k}\cdot\nabla\vec{v}+\\ &\quad+Pm\sqrt{Ta}\,[\vec{B}\cdot\nabla(\nabla\times\vec{B})-(\nabla\times\vec{B})\cdot\nabla\vec{B}].\end{aligned}\tag{2.71}$$

Employing this equation, we can compute vorticity $\vec{\omega}$ and we do not have to take care of pressure Π. However, we need to compute velocity $\vec{v}$ from (2.70) while keeping the condition (2.64) satisfied. This can be easily done using the Fourier transform.

We have also to write the boundary conditions for vorticity. Substitution of (2.33) into (2.70) yields:

$$(\frac{\partial\omega_n}{\partial n}=\omega_t=\omega_s)_{sidewalls,CMB,ICB}=0.\tag{2.72}$$

Chapter 3

Numerical Methods

3.1 Spatial Derivatives Approximation

3.1.1 Finite Difference Method

We will solve the system of equations given in the previous chapter on a regular spatial grid, i.e. we will compute the values of functions and their derivatives at discrete points. Velocity, vorticity and temperature will be computed on the grid with dimensions $(0 \dots K,\ 0 \dots L,\ 0 \dots M)$, that covers the upper box. Magnetic induction will be computed on the grid, that covers the upper box in the same way, but that is also extended in the lower box. Its dimensions are $(0 \dots K,\ 0 \dots L,\ -M_i \dots M)$, where $M_i = \frac{d_i}{d} M$. The dimensionless coordinates (x_k, y_l, z_m) of the point (k, l, m) are

$$\begin{aligned} x_k &= a_x \frac{k}{K}, \\ y_l &= a_y \frac{l}{L}, \\ z_m &= \frac{m}{M}. \end{aligned} \tag{3.1}$$

The spatial derivatives are computed by finite difference scheme. The function $f(x, y, z)$ is approximated near the point (x_k, y_l, z_m) by three polynomials of n-th order (n is even) $P_k^n(x, y_l, z_m)$, $Q_l^n(x_k, y, z_m)$, $R_m^n(x_k, y_l, z)$. Each of the polynomials is given by $n + 1$ points as follows:

$$\begin{aligned} P_k^n(x_i, y_l, z_m) &= f(x_i, y_l, z_m), \quad i = k - \tfrac{n}{2}, \dots, k + \tfrac{n}{2}, \\ Q_l^n(x_k, y_i, z_m) &= f(x_k, y_i, z_m), \quad i = l - \tfrac{n}{2}, \dots, l + \tfrac{n}{2}, \\ R_m^n(x_k, y_l, z_i) &= f(x_k, y_l, z_i), \quad i = m - \tfrac{n}{2}, \dots, m + \tfrac{n}{2}. \end{aligned} \tag{3.2}$$

These conditions yield

$$\begin{aligned} P_k^n(x, y_l, z_m) &= \sum_{i=k-\frac{n}{2}}^{k+\frac{n}{2}} U_{ki}^{n0}(x) f(x_i, y_l, z_m), \\ Q_l^n(x_k, y, z_m) &= \sum_{i=l-\frac{n}{2}}^{l+\frac{n}{2}} V_{li}^{n0}(y) f(x_k, y_i, z_m), \\ R_m^n(x_k, y_l, z) &= \sum_{i=m-\frac{n}{2}}^{m+\frac{n}{2}} W_{mi}^{n0}(z) f(x_k, y_l, z_i). \end{aligned} \tag{3.3}$$

The weighting functions $U_{ki}^{n0}(x)$, $V_{li}^{n0}(y)$ and $W_{mi}^{n0}(z)$ are given by relations

$$\begin{aligned} U_{ki}^{n0}(x) &= \prod_{r=k-\frac{n}{2},r\neq i}^{k+\frac{n}{2}} \frac{x-x_r}{x_i-x_r}, \\ V_{li}^{n0}(y) &= \prod_{r=l-\frac{n}{2},r\neq i}^{l+\frac{n}{2}} \frac{y-y_r}{y_i-y_r}, \\ W_{mi}^{n0}(z) &= \prod_{r=m-\frac{n}{2},r\neq i}^{m+\frac{n}{2}} \frac{z-z_r}{z_i-z_r}. \end{aligned} \tag{3.4}$$

The partial derivatives of $f(x,y,z)$ with respect to x, y, and z at the point (x_k, y_l, z_m) are then approximated by derivation corresponding polynomials

$$\begin{aligned} \tfrac{\partial^p}{\partial x^p} f(x_k,y_l,z_m) &\doteq \sum_{i=k-\frac{n}{2}}^{k+\frac{n}{2}} U_{ki}^{np}(x_k) f(x_i,y_l,z_m), \\ \tfrac{\partial^p}{\partial y^p} f(x_k,y_l,z_m) &\doteq \sum_{i=l-\frac{n}{2}}^{l+\frac{n}{2}} V_{li}^{np}(y_l) f(x_k,y_i,z_m), \\ \tfrac{\partial^p}{\partial z^p} f(x_k,y_l,z_m) &\doteq \sum_{i=m-\frac{n}{2}}^{m+\frac{n}{2}} W_{mi}^{np}(z_m) f(x_k,y_l,z_i). \end{aligned} \tag{3.5}$$

The weights $U_{ki}^{np}(x_k)$, $V_{li}^{np}(y_l)$ and $W_{mi}^{np}(z_m)$ are the values of the p-th partial derivatives of weighting functions (3.4) in the central node. They depend only on the grid coordinates, as given in (3.1) and thus do not have to be computed repeatedly. Moreover, due to the regularity of the grid, the weights do not depend on the point with respect to which they are computed, i.e. they do not depend on k, l and m. The mixed partial derivatives are approximated by the same scheme, applied consequently for different coordinates. In our work we need to compute first order and second order (including some mixed) derivatives. We use the subroutine `weights` from [6].

3.1.2 Discrete Boundary Conditions

To compute the spatial derivatives near the boundaries of the box, we will expand the grid outside it. We will define the function values outside the box antisymmetrically, if the function has zero value at the boundary, or symmetrically, if its derivation (with respect to the coordinate perpendicular

to the boundary) reaches zero at the boundary. For velocity we can write

$$\begin{array}{rclrcl} v^x_{(-k)lm} &=& -v^x_{klm}, & v^x_{(K+k)lm} &=& -v^x_{(K-k)lm}, \\ v^y_{(-k)lm} &=& v^y_{klm}, & v^y_{(K+k)lm} &=& v^y_{(K-k)lm}, \\ v^z_{(-k)lm} &=& v^z_{klm}, & v^z_{(K+k)lm} &=& v^z_{(K-k)lm}, \end{array} \quad k = 0 \ldots \tfrac{n}{2}, \quad l = 0 \ldots L, \quad m = 0 \ldots M, \tag{3.6}$$

$$\begin{array}{rclrcl} v^x_{k(-l)m} &=& v^x_{klm}, & v^x_{k(L+l)m} &=& v^x_{k(L-l)m}, \\ v^y_{k(-l)m} &=& -v^y_{klm}, & v^y_{k(L+l)m} &=& -v^y_{k(L-l)m}, \\ v^z_{k(-l)m} &=& v^z_{klm}, & v^z_{k(L+l)m} &=& v^z_{k(L-l)m}, \end{array} \quad k = 0 \ldots K, \quad l = 0 \ldots \tfrac{n}{2}, \quad m = 0 \ldots M, \tag{3.7}$$

$$\begin{array}{rclrcl} v^x_{kl(-m)} &=& v^x_{klm}, & v^x_{kl(M+m)} &=& v^x_{kl(M-m)}, \\ v^y_{kl(-m)} &=& v^y_{klm}, & v^y_{kl(M+m)} &=& v^y_{kl(M-m)}, \\ v^z_{kl(-m)} &=& -v^z_{klm}, & v^z_{kl(M+m)} &=& -v^z_{kl(M-m)}, \end{array} \quad k = 0 \ldots K, \quad l = 0 \ldots L, \quad m = 0 \ldots \tfrac{n}{2}. \tag{3.8}$$

For vorticity we can write

$$\begin{array}{rclrcl} \omega^x_{(-k)lm} &=& \omega^x_{klm}, & \omega^x_{(K+k)lm} &=& \omega^x_{(K-k)lm}, \\ \omega^y_{(-k)lm} &=& -\omega^y_{klm}, & \omega^y_{(K+k)lm} &=& -\omega^y_{(K-k)lm}, \\ \omega^z_{(-k)lm} &=& -\omega^z_{klm}, & \omega^z_{(K+k)lm} &=& -\omega^z_{(K-k)lm}, \end{array} \quad k = 0 \ldots \tfrac{n}{2}, \quad l = 0 \ldots L, \quad m = 0 \ldots M, \tag{3.9}$$

$$\begin{array}{rclrcl} \omega^x_{k(-l)m} &=& -\omega^x_{klm}, & \omega^x_{k(L+l)m} &=& -\omega^x_{k(L-l)m}, \\ \omega^y_{k(-l)m} &=& \omega^y_{klm}, & \omega^y_{k(L+l)m} &=& \omega^y_{k(L-l)m}, \\ \omega^z_{k(-l)m} &=& -\omega^z_{klm}, & \omega^z_{k(L+l)m} &=& -\omega^z_{k(L-l)m}, \end{array} \quad k = 0 \ldots K, \quad l = 0 \ldots \tfrac{n}{2}, \quad m = 0 \ldots M, \tag{3.10}$$

$$\begin{array}{rclrcl} \omega^x_{kl(-m)} &=& -\omega^x_{klm}, & \omega^x_{kl(M+m)} &=& -\omega^x_{kl(M-m)}, \\ \omega^y_{kl(-m)} &=& -\omega^y_{klm}, & \omega^y_{kl(M+m)} &=& -\omega^y_{kl(M-m)}, \\ \omega^z_{kl(-m)} &=& \omega^z_{klm}, & \omega^z_{kl(M+m)} &=& \omega^z_{kl(M-m)}, \end{array} \quad k = 0 \ldots K, \quad l = 0 \ldots L, \quad m = 0 \ldots \tfrac{n}{2}. \tag{3.11}$$

Temperature is expanded symmetrically at the sidewalls and antisymmetrically at the CMB. At the ICB, we expand antisymmetricaly the non-conductive part of temperature, i.e.

$$T_{(-k)lm} = T_{klm}, \quad T_{(K+k)lm} = T_{(K-k)lm}, \quad k = 0 \ldots \tfrac{n}{2}, \quad l = 0 \ldots L, \quad m = 0 \ldots M, \tag{3.12}$$

$$\begin{array}{c} T_{k(-l)m} = T_{klm}, \quad T_{k(L+l)m} = T_{k(L-l)m}, \\ k = 0 \dots K, \quad l = 0 \dots \frac{n}{2}, \quad m = 0 \dots M, \end{array} \tag{3.13}$$

$$\begin{array}{c} T_{kl(-m)} = 2 - T_{klm}, \quad T_{kl(M+m)} = -T_{kl(M-m)}, \\ k = 0 \dots K, \quad l = 0 \dots L, \quad m = 0 \dots \frac{n}{2}. \end{array} \tag{3.14}$$

The boundary conditions for magnetic induction at the sidewalls and at the bottom of the lower box are again simple

$$\begin{array}{rclrcl} B^x_{(-k)lm} & = & -B^x_{klm}, & B^x_{(K+k)lm} & = & -B^x_{(K-k)lm}, \\ B^y_{(-k)lm} & = & B^y_{klm}, & B^y_{(K+k)lm} & = & B^y_{(K-k)lm}, \\ B^z_{(-k)lm} & = & B^z_{klm}, & B^z_{(K+k)lm} & = & B^z_{(K-k)lm}, \\ \multicolumn{6}{c}{k = 0 \dots \frac{n}{2}, \quad l = 0 \dots L, \quad m = -M_i \dots M,} \end{array} \tag{3.15}$$

$$\begin{array}{rclrcl} B^x_{k(-l)m} & = & B^x_{klm}, & B^x_{k(L+l)m} & = & B^x_{k(L-l)m}, \\ B^y_{k(-l)m} & = & -B^y_{klm}, & B^y_{k(L+l)m} & = & -B^y_{k(L-l)m}, \\ B^z_{k(-l)m} & = & B^z_{klm}, & B^z_{k(L+l)m} & = & B^z_{k(L-l)m}, \\ \multicolumn{6}{c}{k = 0 \dots K, \quad l = 0 \dots \frac{n}{2}, \quad m = -M_i \dots M,} \end{array} \tag{3.16}$$

$$\begin{array}{rcl} B^x_{kl(-M_i-m)} & = & -B^x_{kl(-M_i+m)}, \\ B^y_{kl(-M_i-m)} & = & -B^y_{kl(-M_i+m)}, \\ B^z_{kl(-M_i-m)} & = & B^z_{kl(-M_i+m)}, \\ \multicolumn{3}{c}{k = 0 \dots K, \quad l = 0 \dots L, \quad m = 0 \dots \frac{n}{2}.} \end{array} \tag{3.17}$$

The values of magnetic induction above the CMB should be computed according to (2.42). The horizontal dimensions of the grid, where $\vec{B}$ is computed, are $(0 \dots K, 0 \dots L)$. Therefore the Fourier series used in (2.40) – (2.42) must be replaced by discrete Fourier transform. We must also take into account the relations (3.1) between grid coordinates and corresponding indices. Then we can write

$$\vec{B}_{klm} = \frac{1}{(K+1)(L+1)} \sum_{p,q=0}^{K,L} \hat{\vec{B}}_{pqm} e^{[-2\pi i(\frac{pk}{K+1} + \frac{ql}{L+1})]}, \tag{3.18}$$

$$\{-4\pi^2[(\frac{K}{K+1}\frac{p}{a_x})^2 + (\frac{L}{L+1}\frac{q}{a_y})^2] + M^2\frac{\partial^2}{\partial m^2}\}\hat{\vec{B}}_{pqm} = 0, \tag{3.19}$$

$$\begin{array}{c} \hat{\vec{B}}_{pq(M+m)} = \hat{\vec{B}}_{pqM} e^{[-2\pi\sqrt{(\frac{K}{K+1}\frac{p}{a_x})^2 + (\frac{L}{L+1}\frac{q}{a_y})^2}\,\frac{m}{M}]}, \\ p = 0 \dots K, \quad q = 0 \dots L, \quad m = 0 \dots \frac{n}{2}. \end{array} \tag{3.20}$$

It is not quite correct to derivate with respect to m, which is a discrete index, but this notation allowed us to express the exponent in (3.20). Thus,

we compute the 2D discrete Fourier transform $\hat{\vec{B}}_{pqM}$ of magnetic induction at the top of the box $\vec{B}_{klM}$, then we expand it above the CMB by applying the exponential decay (3.20) and finally we return to the spatial domain by the inverse discrete Fourier transform (3.18) applied in $\frac{n}{2}$ layers above the CMB.

3.2 Discrete Fourier Transform

We use the discrete Fourier transform to compute velocity of the fluid $\vec{v}$ from (2.70). Numerically, both the direct and the inverse Fourier transforms are realized with fast Fourier transform procedure for 3D real functions `rlft3` from [12]. First, let us write the inverse Fourier transforms of velocity and vorticity

$$\vec{v}_{klm} = \frac{1}{(K+1)(L+1)(M+1)} \sum_{p,q,r=0}^{K,L,M} \hat{\vec{v}}_{pqr} e^{[-2\pi i(\frac{pk}{K+1}+\frac{ql}{L+1}+\frac{rm}{M+1})]}, \quad (3.21)$$

$$\vec{\omega}_{klm} = \frac{1}{(K+1)(L+1)(M+1)} \sum_{p,q,r=0}^{K,L,M} \hat{\vec{\omega}}_{pqr} e^{[-2\pi i(\frac{pk}{K+1}+\frac{ql}{L+1}+\frac{rm}{M+1})]}. \quad (3.22)$$

The definition of vorticity (2.70) yields

$$\nabla \cdot \vec{\omega} = 0, \quad (3.23)$$

which can be rewritten in the spectral domain, using also (3.1), as

$$\frac{K}{K+1}\frac{p}{a_x}\hat{\omega}^x_{pqr} + \frac{L}{L+1}\frac{q}{a_y}\hat{\omega}^y_{pqr} + \frac{M}{M+1} r \hat{\omega}^z_{pqr} = 0. \quad (3.24)$$

Therefore it is not necessary to compute all three components of vorticity from (2.71), but one of them, let it be ω_z, can be computed from its discrete Fourier transform given by equation

$$\hat{\omega}^z_{pqr} = -\frac{M+1}{M}\frac{1}{r}\left(\frac{K}{K+1}\frac{k}{a_x}\hat{\omega}^x_{pqr} + \frac{L}{L+1}\frac{q}{a_y}\hat{\omega}^y_{pqr}\right). \quad (3.25)$$

Now, let us rewrite the definition of vorticity (2.70) in the spectral form:

$$\begin{aligned} \hat{\omega}^x_{pqr} &= 2\pi i\left(\tfrac{M}{M+1} r \hat{v}^y_{pqr} - \tfrac{L}{L+1}\tfrac{q}{a_y}\hat{v}^z_{pqr}\right), \\ \hat{\omega}^y_{pqr} &= 2\pi i\left(\tfrac{K}{K+1}\tfrac{p}{a_x}\hat{v}^z_{pqr} - \tfrac{M}{M+1} r \hat{v}^x_{pqr}\right), \\ \hat{\omega}^z_{pqr} &= 2\pi i\left(\tfrac{L}{L+1}\tfrac{q}{a_y}\hat{v}^x_{pqr} - \tfrac{K}{K+1}\tfrac{p}{a_x}\hat{v}^y_{pqr}\right). \end{aligned} \quad (3.26)$$

But we can also consider (3.26) as a system for solving $\hat{\vec{v}}_{pqr}$:

$$\begin{array}{rcrcrcl} \frac{L}{L+1}\frac{q}{a_y}\,\hat{v}^x_{pqr} & - & \frac{K}{K+1}\frac{p}{a_x}\,\hat{v}^y_{pqr} & & & = & \frac{\hat{\omega}^z_{pqr}}{2\pi i}, \\ -\frac{M}{M+1}\,r\,\hat{v}^x_{pqr} & & & + & \frac{K}{K+1}\frac{p}{a_x}\,\hat{v}^z_{pqr} & = & \frac{\hat{\omega}^y_{pqr}}{2\pi i}, \\ & & \frac{M}{M+1}\,r\,\hat{v}^y_{pqr} & - & \frac{L}{L+1}\frac{q}{a_y}\,\hat{v}^z_{pqr} & = & \frac{\hat{\omega}^x_{pqr}}{2\pi i}. \end{array} \tag{3.27}$$

This system is not regular, because its determinant is zero. But velocity must also satisfy (2.64), which can be written in the spectral domain as

$$\frac{K}{K+1}\frac{k}{a_x}\,\hat{v}^x_{pqr} + \frac{L}{L+1}\frac{l}{a_y}\,\hat{v}^y_{pqr} + \frac{M}{M+1}\,r\,\hat{v}^z_{pqr} = 0. \tag{3.28}$$

Replacing one of the equations in (3.27) by (3.28) gives a well determined linear system of equations which can be easily solved:

$$\begin{array}{rcl} \hat{v}^x_{pqr} & = & \frac{i(\frac{M}{M+1}\,r\,\hat{\omega}^y_{pqr} - \frac{L}{L+1}\frac{q}{a_y}\,\hat{\omega}^z_{pqr})}{2\pi[(\frac{K}{K+1}\frac{p}{a_x})^2+(\frac{L}{L+1}\frac{q}{a_y})^2+(\frac{M}{M+1}\,r)^2]}, \\ \hat{v}^y_{pqr} & = & \frac{i(\frac{K}{K+1}\frac{p}{a_x}\,\hat{\omega}^z_{pqr} - \frac{M}{M+1}\,r\,\hat{\omega}^x_{pqr})i}{2\pi[(\frac{K}{K+1}\frac{p}{a_x})^2+(\frac{L}{L+1}\frac{q}{a_y})^2+(\frac{M}{M+1}\,r)^2]}, \\ \hat{v}^z_{pqr} & = & \frac{i(\frac{L}{L+1}\frac{q}{a_y}\,\hat{\omega}^x_{pqr} - \frac{K}{K+1}\frac{p}{a_x}\,\hat{\omega}^y_{pqr})}{2\pi[(\frac{K}{K+1}\frac{p}{a_x})^2+(\frac{L}{L+1}\frac{q}{a_y})^2+(\frac{M}{M+1}\,r)^2]}. \end{array} \tag{3.29}$$

3.3 Time Evolution

We use the modified Euler method, which is a special case of the 2^{nd} order Runge-Kutta method to compute the time evolution of equations (2.66), (2.67) and (2.71). As we have showed in the previous section, in each time step we can compute the velocity field from vorticity, thus we can formally write

$$\frac{\partial \vec{B}}{\partial t} = \vec{F}_1(\vec{B}, \vec{v}(\vec{\omega})) = \vec{F}_1(\vec{B}, \vec{\omega}), \tag{3.30}$$

$$\frac{\partial T}{\partial t} = F_2(T, \vec{B}, \vec{v}(\vec{\omega})) = F_2(T, \vec{B}, \vec{\omega}), \tag{3.31}$$

$$\frac{\partial \vec{\omega}}{\partial t} = \vec{F}_3(T, \vec{B}, \vec{v}(\vec{\omega}), \vec{\omega}) = \vec{F}_3(T, \vec{B}, \vec{\omega}). \tag{3.32}$$

Then magnetic induction, temperature and vorticity in the $(n+1)^{\text{th}}$ time step will be

$$\vec{B}_{n+1} = \vec{B}_n + \frac{\Delta t}{2}(\vec{F}_1(\vec{B}_n, \vec{\omega}_n) + \vec{F}_1(\vec{B}', \vec{\omega}')), \tag{3.33}$$

$$T_{n+1} = T_n + \frac{\Delta t}{2}(F_2(T_n, \vec{B}_n, \vec{\omega}_n) + F_2(T', \vec{B}', \vec{\omega}')), \tag{3.34}$$

$$\vec{\omega}_{n+1} = \vec{\omega}_n + \frac{\Delta t}{2}(\vec{F}_3(T_n, \vec{B}_n, \vec{\omega}_n) + \vec{F}_3(T', \vec{B}', \vec{\omega}')), \tag{3.35}$$

where

$$\vec{B}' = \vec{B}_n + \Delta t\, \vec{F}_1(\vec{B}_n, \vec{\omega}_n), \tag{3.36}$$

$$T' = T_n + \Delta t\, F_2(T_n, \vec{B}_n, \vec{\omega}_n), \tag{3.37}$$

$$\vec{\omega}' = \vec{\omega}_n + \Delta t\, \vec{F}_3(T_n, \vec{B}_n, \vec{\omega}_n). \tag{3.38}$$

The time step Δt must satisfy the Courant-Friedrichs-Levy criterion. Depending on the parameters describing the system and on velocity, it is given by one of several different terms in the evolutionary equations. The equation of magnetic induction (2.67) yields two conditions,

$$\Delta t < \Delta t_1 = \min[dx^2, dy^2, dz^2] \tag{3.39}$$

and

$$\Delta t < \Delta t_2 = \min[\frac{dx}{v_x^{max}}, \frac{dy}{v_y^{max}}, \frac{dz}{v_z^{max}}], \tag{3.40}$$

where $dx = \frac{a_x}{K}$, $dy = \frac{a_y}{L}$ and $dz = \frac{1}{M}$ are the grid distances and v_x^{max}, v_y^{max} and v_z^{max} denote the maximum velocity components. The equation governing the evolution of vorticity (2.71) also limits the time step by two relations. The first one is identical with (3.40), while the second one is

$$\Delta t < \Delta t_3 = \frac{1}{Pm} \min[dx^2, dy^2, dz^2]. \tag{3.41}$$

The equation for temperature (2.66) also requires (3.40) to be satisfied, together with

$$\Delta t < \Delta t_4 = \frac{Pr}{Pm} \min[dx^2, dy^2, dz^2]. \tag{3.42}$$

Therefore, the final formula for the time step is

$$\Delta t = t_c \min[\Delta t_1, \Delta t_2, \Delta t_3, \Delta t_4], \tag{3.43}$$

where $t_c < 1$ must be set experimentally.

Chapter 4

Results

4.1 Parameters of the Models

Behaviour of the system described in *Chapter 2* depends on the choice of physical and numerical parameters of the model. Tab. 4.1 shows the summary of physical parameters of the Earth's outer and inner core. Some of them, e.g. the dimensions of the outer and the inner core, the radial dependency of density or gravitational acceleration are well known from the PREM model. The thermodynamic and physico-chemical parameters are much more uncertain. Their values depend on the chemical composition of the core and are estimated from theoretical assumptions and from high pressure experiments. Especially the estimates of kinematic viscosity and internal heating rate may vary in range of orders.

Parameter	**Symbol**	**Value**
Well determined parameters		
outer core radius	R_{OC}	$3.48\ 10^6$ m
inner core radius	R_{IC}	$1.22\ 10^6$ m
magnitude of Earth's rotation	Ω	$7.3\ 10^{-5}$ s^{-1}
reference density at T_0 (i.e. at the CMB)	ρ_0	$9.9\ 10^3$ kg m^{-3}
gravitational acceleration at the CMB	g_{CMB}	10.68 m s^{-2}
gravitational acceleration at the ICB	g_{ICB}	4.40 m s^{-2}
Poorly determined parameters		
temperature at the CMB	T_0	4000 K
temperature drop between ICB and CMB	δT	1300 K
thermal expansivity at the CMB	α_{CMB}	$1.76\ 10^{-5}$ K^{-1}
thermal expansivity at the ICB	α_{ICB}	$0.98\ 10^{-5}$ K^{-1}
specific heat at a const. pressure at the CMB	$C_{p,CMB}$	848 m^2 s^{-2} K^{-1}
specific heat at a const. pressure at the ICB	$C_{p,ICB}$	826 m^2 s^{-2} K^{-1}
magnetic diffusivity	λ	10^0 m^2 s^{-1}
kinematic viscosity	ν	$10^{-7} - 10^3$ m^2 s^{-1}
thermal diffusivity	κ	10^{-6} m^2 s^{-1}
internal heating rate	Q	$0 - 10^{12}$ kg m^{-1} s^{-3}

Table 4.1: Physical parameters of the Earth's interior, according to [2, 5, 14].

In our model, we use the set of seven dimensionless numbers, that characterize the system. Prandtl (2.59) and Prandtl magnetic (2.60) numbers compare the diffusion rates of velocity, temperature and magnetic field. Rayleigh number (2.61) determines the thermal buoyancy. Taylor number (2.62) compares the Coriolis force with the diffusion of velocity. Dissipation number affects the adiabatic, viscous and Joule heating. The ratio $\frac{T_0}{\delta T}$ is involved only in the adiabatic heating and the dimensionless internal heating rate Q represents radioactive heat sources in the outer core. Tab. 4.2 contains the possible values of these parameters in the Earth based on the estimates in Tab. 4.1 (note, that the dimensionless internal heating rate Q differs from the SI value) and the values, that we have chosen for our cases. The Earth's rotation vector is parallel with the z-axis, as we have stated in *Chapter 1*, i.e. $\vec{k} = (0, 0, 1)$.

Parameter	**Earth**	**Case I**	**Case II**	**Case III**
Pr	$10^{-1} - 10^{9}$	1	1	1
Pm	$10^{-7} - 10^{3}$	1	1	1
Ra	$10^{21} - 10^{31}$	10^{4}	10^{4}	10^{4}
Ta	$10^{11} - 10^{31}$	10^{4}	10^{6}	10^{4}
Dn	0.2	0	0	0.2
$\frac{T_0}{\delta T}$	3	0	0	4
Q	$0 - 10^{14}$	0	0	0

Table 4.2: Dimensionless parameters of the Earth and the computed cases.

We have evolved the system for three different sets of parameters. In Case I we have simplified the energy equation by neglecting the viscous and ohmic dissipation and the adiabatic term. In Case II we have increased the Taylor number, i.e. the Coriolis and Lorentz forces. The most complex Case III includes the effects of dissipation and adiabatic heating. The values of Ra and Ta for the Earth are far behind our computational reach. As we will see later in this chapter, our choice of the Rayleigh number corresponds to the steady state of the flow. We have also unified the magnitude of diffusive terms for velocity, temperature and magnetic induction by setting the Prandtl and Prandtl magnetic numbers to the same value in order to allow the velocity and temperature to evolve at the same time scale as the magnetic induction. We have neglected the internal heating in the core.

The numerical parameters are the same for all three cases and are summarized in Tab. 4.3. The fast Fourier transform algorithm limited our choice of number of grid points in the upper box to integer powers of two. The

choice of relative horizontal sizes of the box means, that the vertical resolution of the model is twice the horizontal one. We used the 8^{th} order finite differences scheme, so we had to increase the dimensions of all fields by 4 at each side. Our FORTRAN code required about 80 MB of memory with single (4 bytes) representation of real numbers and one time step took 1 – 2 minutes on a HP workstation.

Parameter	**Symbol**	**Value**
horizontal grid dimensions	$(0 \dots K, 0 \dots L)$	$(0 \dots 63, 0 \dots 63)$
vertical grid dimension of the upper box	$(0 \dots M)$	$(0 \dots 63)$
vertical grid dimension of the lower box	$(-M_i \dots 0)$	$(-41 \dots 0)$
relative horizontal sizes of boxes	a_x, a_y	2, 2
finite differences order	n	8
time step factor	t_c	0.2

Table 4.3: Numerical parameters of models.

4.2 Integral Quantities

In this section we will introduce several physical quantities and numbers which are usefull in the description of physical and numerical behaviour of the system. By the word "integral" we mean that they are defined globally, as an integral or average over the entire computational domain.

The kinetic energy of the fluid in the outer core is defined by relation

$$E_k = \frac{1}{2} \int\limits_{OC} \rho \vec{v} \cdot \vec{v} \, dV \doteq \frac{\rho_0}{2} \int\limits_{OC} \vec{v} \cdot \vec{v} \, dV, \tag{4.1}$$

where we neglect the changes of density with respect to the reference state. Similarly, we define the energy of the magnetic field in the entire core as

$$E_m = \frac{1}{2\mu_0} \int\limits_{IC+OC} \vec{B} \cdot \vec{B} \, dV. \tag{4.2}$$

Note, that the quantities in these definitions are in SI units. We will scale the energy (kinetic as well as magnetic) as follows:

$$E = \rho_0 d\lambda^2 \, E'. \tag{4.3}$$

Now, using the dimensionless velocity, magnetic induction, energy and volume (primes are again omitted) we can write

$$E_k = \frac{1}{2} \int\limits_{OC} \vec{v} \cdot \vec{v}\, dV \tag{4.4}$$

and

$$E_m = \frac{Pm\sqrt{Ta}}{2} \int\limits_{IC+OC} \vec{B} \cdot \vec{B}\, dV. \tag{4.5}$$

The discrete forms of (4.4) and (4.5) are

$$E_k = \frac{a_x\, a_y}{2\, K\, L\, M} \sum_{k,l,m=0}^{K,L,M} v_{klm}^2, \tag{4.6}$$

$$E_m = \frac{Pm\sqrt{Ta}\, a_x\, a_y}{2\, K\, L\, (M + M_i)} \sum_{k,l=0,\, m=-M_i}^{K,L,M} B_{klm}^2. \tag{4.7}$$

To compare the importance of dissipative terms in Case III, we will define dimensionless numbers Q_V, Q_A and Q_J that describe average viscous, adiabatic and Joule heating:

$$\begin{aligned} Q_V &= \frac{Dn\, Pr}{Ra\, Pm\, V_{OC}} \int\limits_{OC} \overleftrightarrow{\sigma} : \nabla \vec{v}\, dV = \\ &= \frac{Dn\, Pr}{Ra\, Pm\, K\, L\, M} \sum_{k,l,m=0}^{K,L,M} (\overleftrightarrow{\sigma} : \nabla \vec{v})_{klm}, \end{aligned} \tag{4.8}$$

$$\begin{aligned} Q_A &= \frac{Dn}{V_{OC}} \int\limits_{OC} |(T + \frac{T_0}{\delta T}) \vec{v} \cdot \vec{e}_z|\, dV = \\ &= \frac{Dn}{K\, L\, M} \sum_{k,l,m=0}^{K,L,M} |(T_{klm} + \frac{T_0}{\delta T}) v_{klm}^z|, \end{aligned} \tag{4.9}$$

$$\begin{aligned} Q_J &= \frac{Dn\, Pr\sqrt{Ta}}{Ra\, Pm\, V_{OC}} \int\limits_{OC} (\nabla \times \vec{B})^2\, dV = \\ &= \frac{Dn\, Pr\sqrt{Ta}}{Ra\, Pm\, K\, L\, M} \sum_{k,l,m=0}^{K,L,M} (\nabla \times \vec{B})_{klm}^2. \end{aligned} \tag{4.10}$$

We will also use dimensionless numbers F_B, F_C and F_L as measures of thermal buoyancy, Coriolis and Lorentz forces acting in the fluid,

$$\begin{aligned} F_B &= \frac{(Pm)^2\, Ra}{Pr\, V_{OC}} \int\limits_{OC} |T|\, dV = \\ &= \frac{(Pm)^2\, Ra}{Pr\, K\, L\, M} \sum_{k,l,m=0}^{K,L,M} |T_{klm}|, \end{aligned} \tag{4.11}$$

$$\begin{aligned} F_C &= \frac{Pm\,\sqrt{Ta}}{V_{OC}} \int\limits_{OC} |\vec{k} \times \vec{v}|\, dV = \\ &= \frac{Pm\,\sqrt{Ta}}{K\, L\, M} \sum_{k,l,m=0}^{K,L,M} \sqrt{(v^x_{klm})^2 + (v^y_{klm})^2}, \end{aligned} \tag{4.12}$$

$$\begin{aligned} F_L &= \frac{Pm\,\sqrt{Ta}}{V_{OC}} \int\limits_{OC} |(\nabla \times \vec{B}) \times \vec{B}|\, dV = \\ &= \frac{Pm\,\sqrt{Ta}}{K\, L\, M} \sum_{k,l,m=0}^{K,L,M} |[(\nabla \times \vec{B}) \times \vec{B}]_{klm}|. \end{aligned} \tag{4.13}$$

To check the evolution of $\nabla \cdot \vec{B}$ in time we introduce number D_B as an average of absolute value of (dimensionless) magnetic induction divergence over the entire core:

$$\begin{aligned} D_B &= \frac{1}{V_{IC} + V_{OC}} \int\limits_{IC+OC} |\nabla \cdot B|\, dV = \\ &= \frac{1}{K\, L\, (M + M_i)} \sum_{k,l=0,\, m=-M_i}^{K,L,M} |(\nabla \cdot \vec{B})_{klm}|. \end{aligned} \tag{4.14}$$

4.3 Case I

As an initial condition of the simulation we used the temperature and velocity fields corresponding to the non-magnetic stationary flow (with the same Prandtl, Rayleigh and Taylor numbers) and we imposed weak homogeneous magnetic field in the vertical direction. We evolved the system until the dimensionless time reached $t = 0.12$.

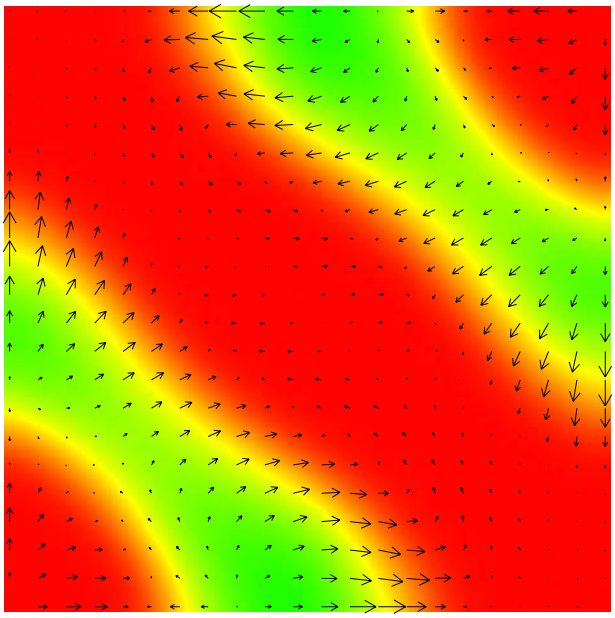

(a)

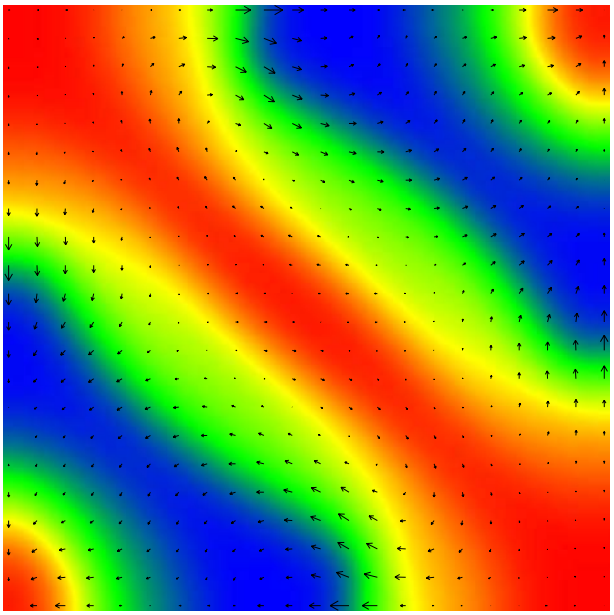

(b)

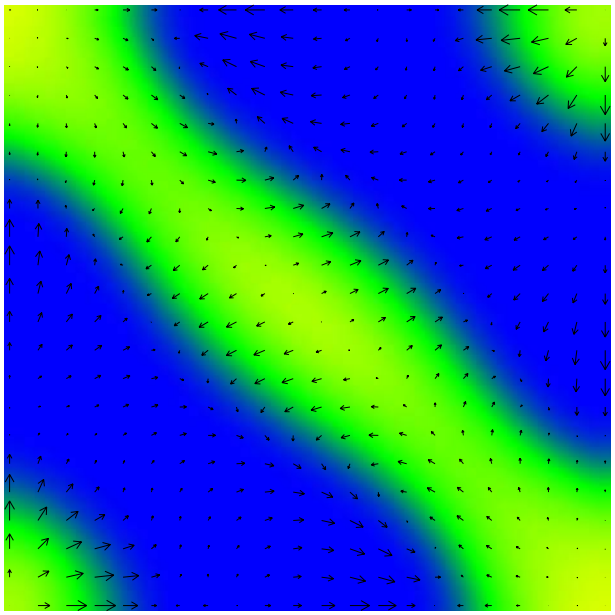

(c)

Figure 4.1: Case I. Temperature and projection of velocity in horizontal planes xy for (a) $m = 1$, (b) $m = 32$, (c) $m = 62$.

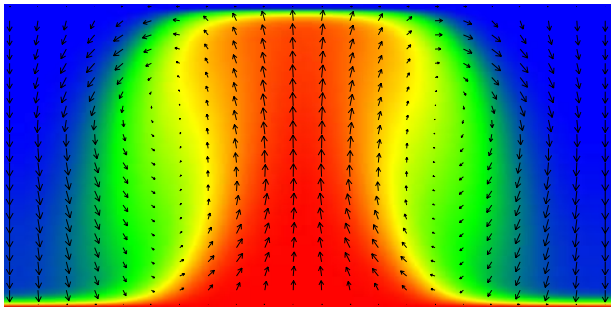

Figure 4.2: Case I. Temperature and projection of velocity in vertical plane yz for $k = 32$.

Figures 4.1 and 4.2 show temperature and velocity in different cross-sections through the box at the end of the simulation. Temperature is represented by the coloured background (using a symmetrical blue–green–red palette), the black arrows correspond to velocity, horizontal and vertical components use separate scalings, but uniform in the entire box (independent on the position of cross-section). The flow structure shows a high degree of symmetry with one large hot plume across the box and two small hot plumes in the opposite corners. The fluid descends back to the bottom in two cold bands between the hot upwellings. Maximum velocities in the horizontal direction are about 35 and are concentrated above the bottom

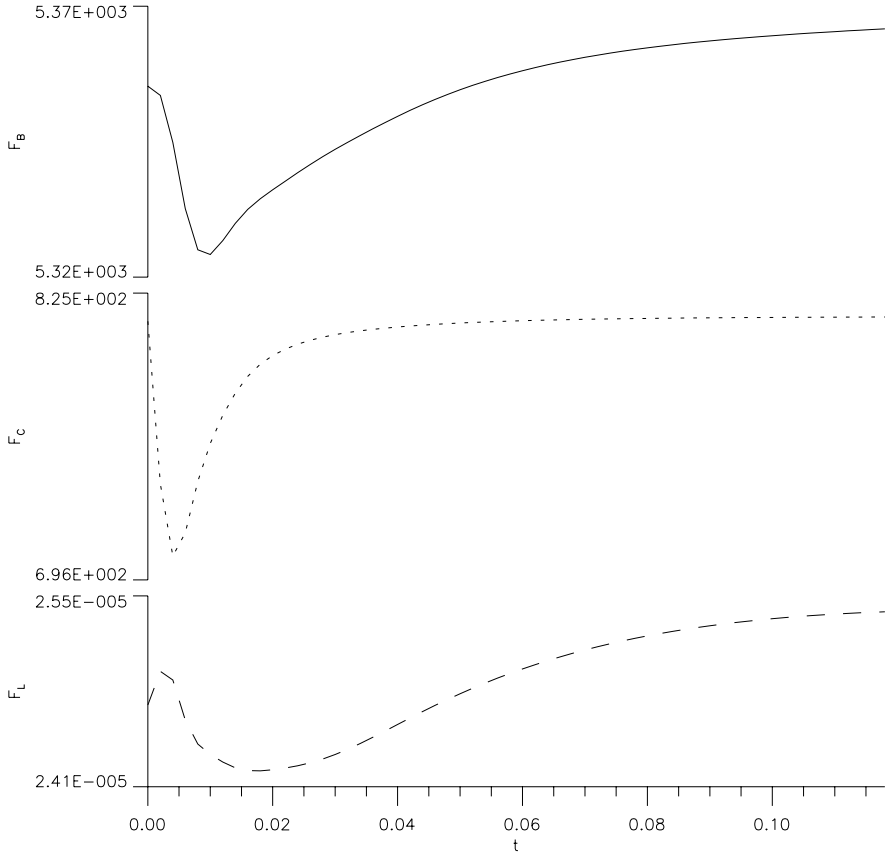

Figure 4.3: Case I. Time evolution of average buoyancy force F_B (solid line), the Coriolis force F_C (dotted line) and the Lorentz force F_L (dashed line).

and below the top of the box, where the material enters and leaves the hot upwellings and cold downwellings. The vertical velocity reaches the maximum values of 85 in both directions. The Coriolis force, which is about 15% of thermal buoyancy force (see Fig. 4.3), screws horizontal velocity in the clockwise direction. The Lorentz force is weak and has no influence on the flow structure. The flow of the fluid is very close to its steady state with only small changes of velocity and temperature fields in time. This fact is in agreement with results obtained in [9].

The force lines of magnetic induction at the end of the simulation are shown in Fig. 4.4, while Fig. 4.5 represents horizontal magnetic field in cross-sections through both the lower (inner core) and upper (outer core) box. We can see, that the field keeps its dominantly vertical direction, the maximum values of B_z are about 0.0039, while the horizontal field reaches values up to 0.0018. In the areas where the flow is mainly vertical, i.e. inside the upwellings and the downwellings, magnetic induction remains also vertical because $(\vec{v} \times \vec{B}) \doteq 0$ there.

The horizontal flow of the fluid invokes horizontal screwing of the magnetic induction lines. However, the horizontal direction of magnetic induc-

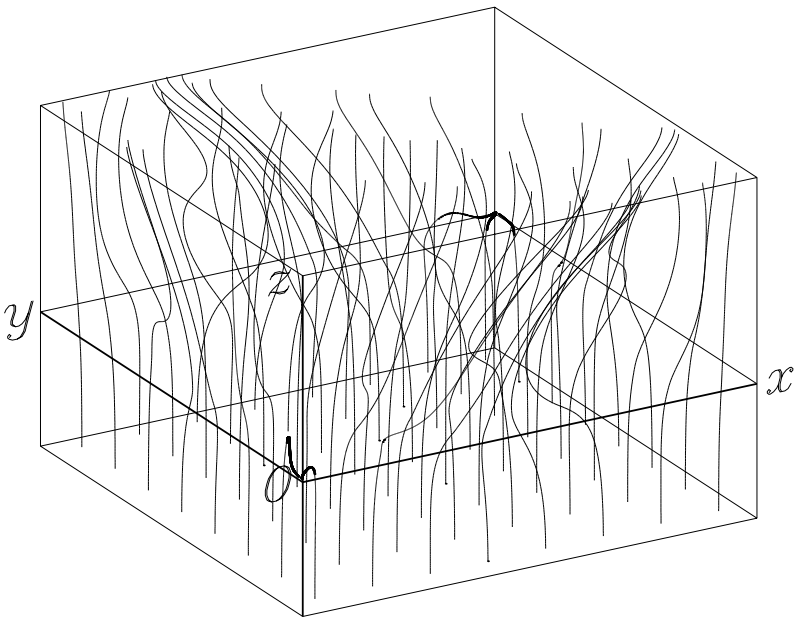

Figure 4.4: Case I. Magnetic induction.

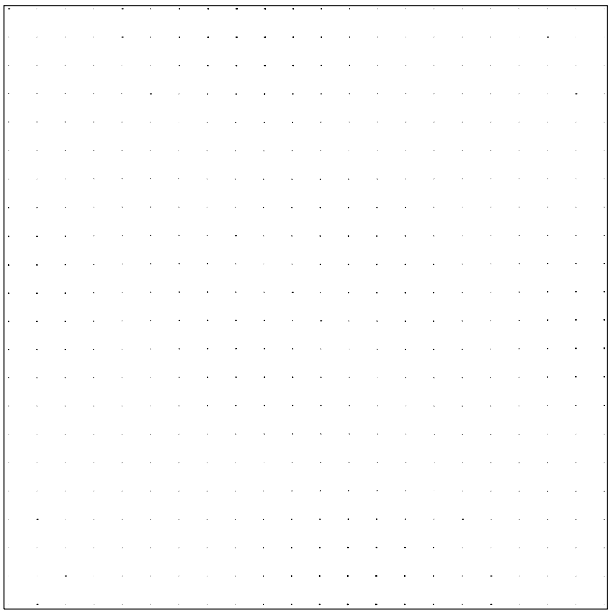

(a)

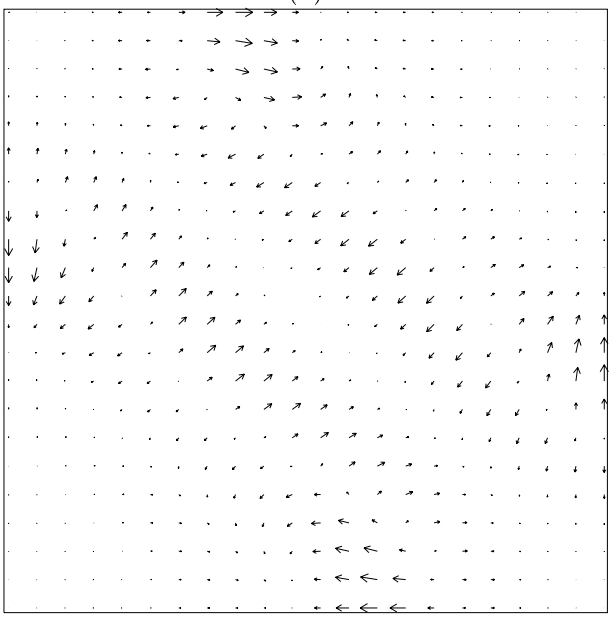

(b)

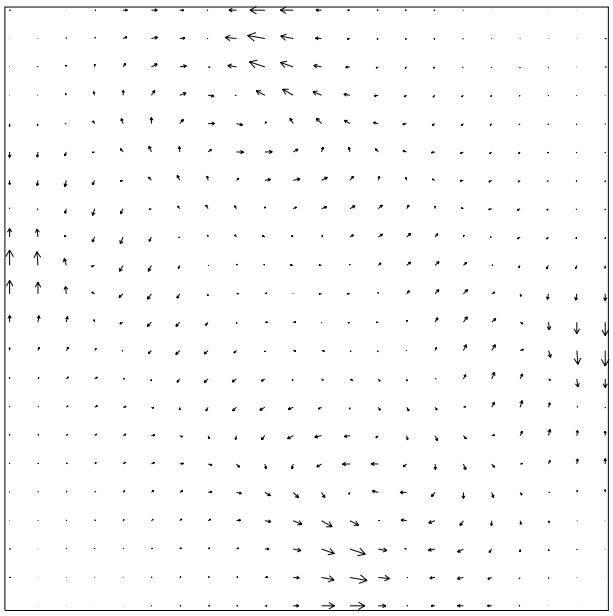

(c)

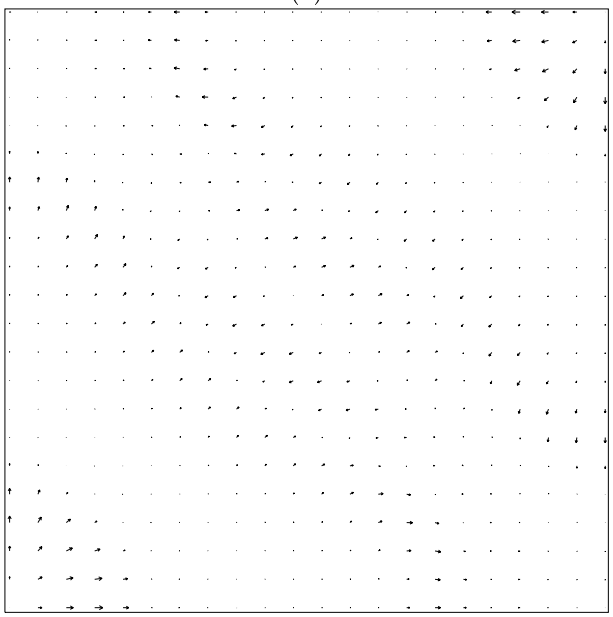

(d)

Figure 4.5: Case I. Projection of magnetic induction in horizontal planes xy for (a) $m = -20$, (b) $m = 1$, (c) $m = 32$, (d) $m = 62$.

tion does not always agree with the horizontal direction of velocity as it would correspond to the drift of the magnetic field by the fluid. How can we explain this discrepancy? Both the velocity and magnetic fields are solenoidal, i.e. they satisfy (2.18) and (2.64). But the velocity is restrained in the box by the impermeable and free-slip boundary conditions, while the magnetic field enters the outer core box from the inner core at the bottom and leaves it to the mantle at the top. Therefore the vertical component of the velocity significantly changes in the box in contrast to the vertical magnetic field, which undergoes only minor changes. Relations (2.18) and (2.64) then imply different constraints on the horizontal components of velocity and magnetic field. In the lower box, where only the diffusive term applies, the horizontal magnetic field rapidly decreases with increasing depth.

Our model represents so called "weak field dynamo" with the magnetic energy being several orders lower than the kinetic energy (see Fig. 4.6). Although the magnetic energy has slightly increased during the simulation, it remains eight orders below the kinetic energy.

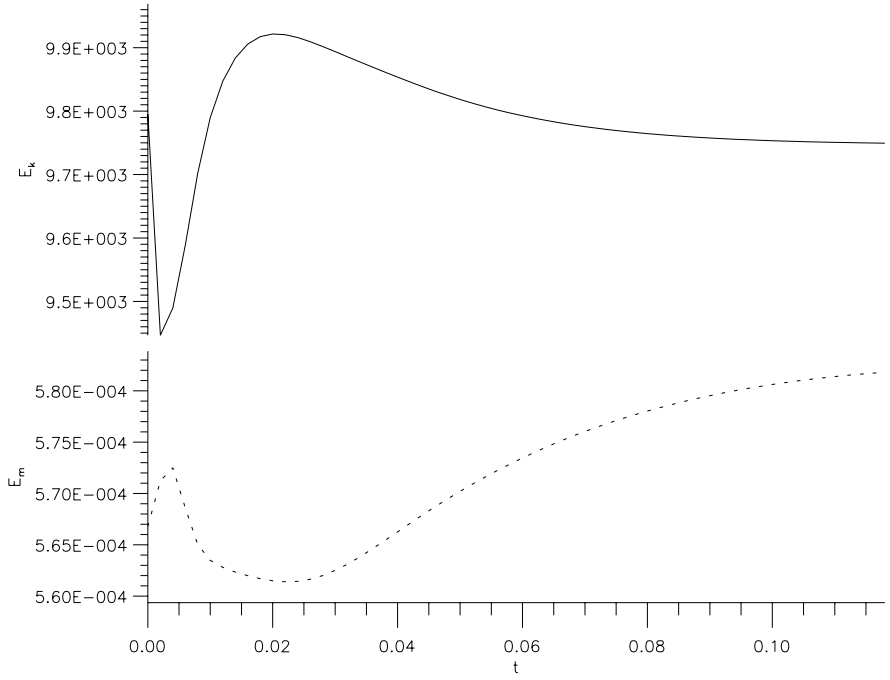

Figure 4.6: Case I. Time evolution of the kinetic energy of the fluid and the energy of the magnetic field.

4.4 Case II

We have started the second model from the stationary solution of the flow and vertical homogeneous magnetic field again and evolved it for $t = 0.14$.

The flow structure at the end of the simulation is shown in Figs. 4.8 and 4.9. The fluid flows up in two large, band-like upwellings parallel with the x-axis and situated by the sidewalls of the box. One broad, cold downwelling between the hot areas transports the fluid back to the bottom of the box. The horizontal velocities are less than 8.5 in the x-direction and 18 in the y-direction, as the symmetry with respect to the diagonal, that we observed

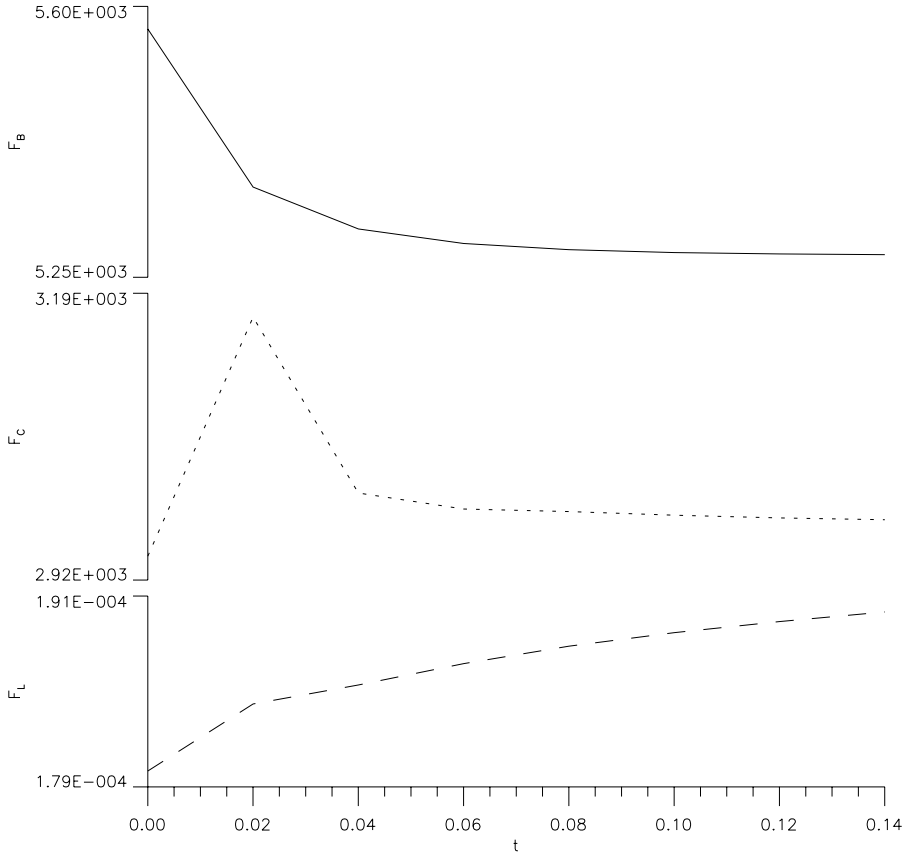

Figure 4.7: Case II. Time evolution of average buoyancy force F_B (solid line), the Coriolis force F_C (dotted line) and the Lorentz force F_L (dashed line).

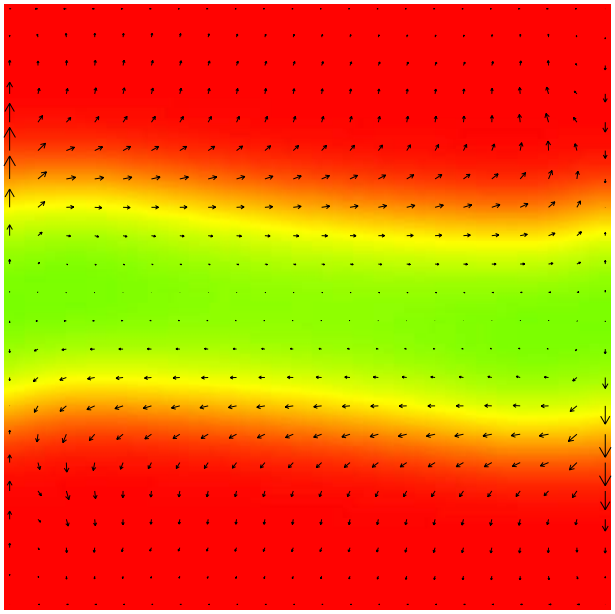

(a)

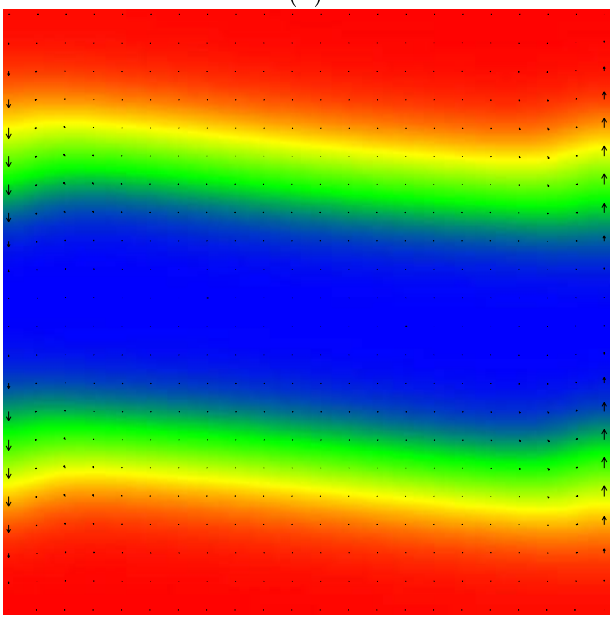

(b)

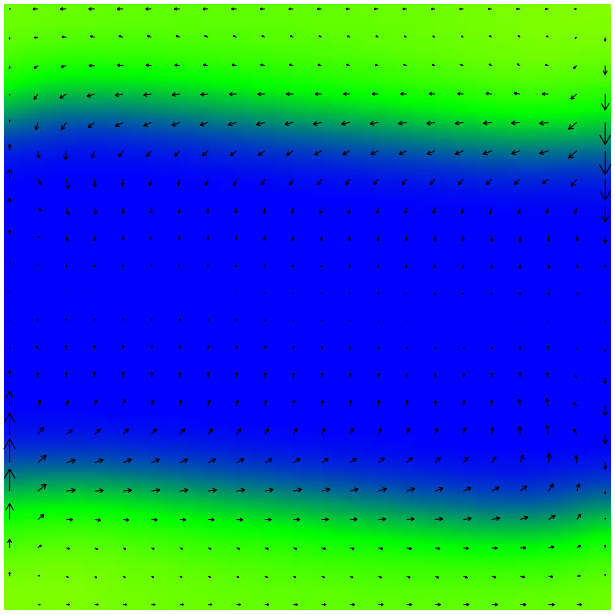

(c)

Figure 4.8: Case II. Temperature and projection of velocity in horizontal planes xy for (a) $m = 1$, (b) $m = 32$, (c) $m = 62$.

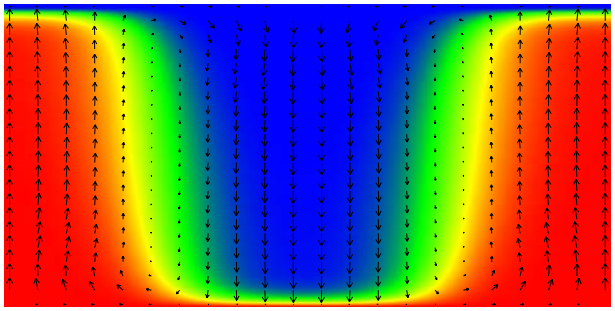

Figure 4.9: Case II. Temperature and projection of velocity in vertical plane yz for $k = 32$.

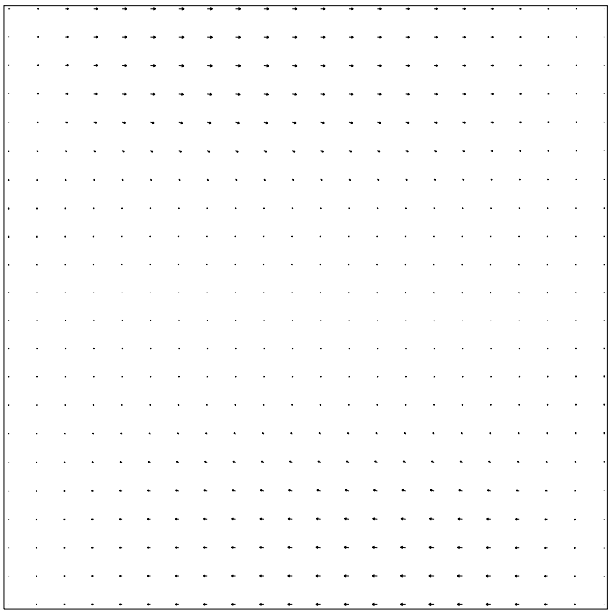

(a)

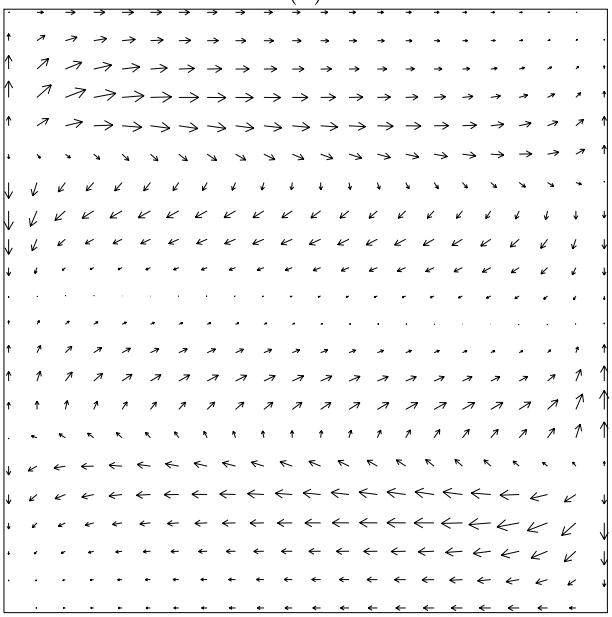

(b)

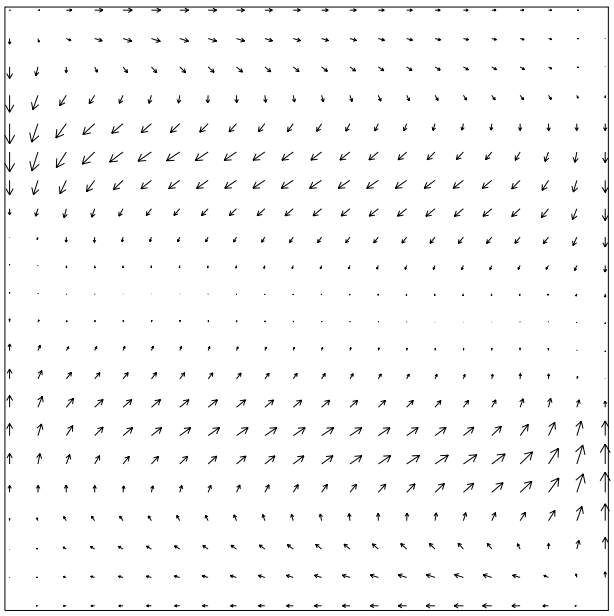

(c)

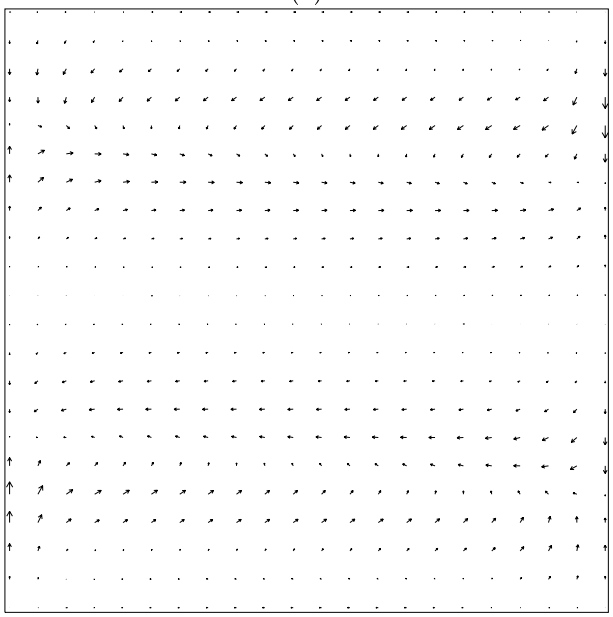

(d)

Figure 4.10: Case II. Projection of magnetic induction in horizontal planes xy for (a) $m = -20$, (b) $m = 1$, (c) $m = 32$, (d) $m = 62$.

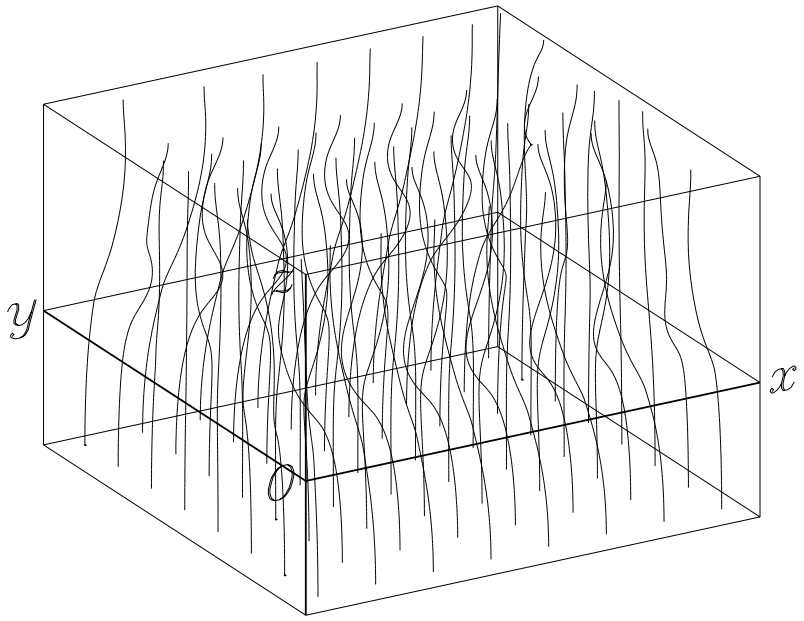

Figure 4.11: Case II. Magnetic induction.

in the previous case, was replaced by the symmetry of the temperature and antisymmetry of the flow with respect to the plane $y = \frac{a_y}{2}$. The vertical velocities do not exceed 50. The effect of the Coriolis force is now of the same order as the buoyancy (see Fig. 4.7). At the bottom and the top of the box we can see the screwing of high velocities in the y-direction to the right. The ratio of Lorentz force to the buoyancy is larger, than in the previous case, but the magnetic field is still too weak to act significantly on the fluid.

The structure of the magnetic field is similar to Case I. Horizontal motions lead to deformations of dominantly vertical force lines (see Fig. 4.11). The cross-sections (Fig. 4.10) show, that the horizontal magnetic field has similar antisymmetry as the horizontal velocity field, although it does not copy its structure. The maximum values reached 0.00041 in the x-direction, 0.00033 in the y-direction and 0.0024 in the z-direction.

The time evolution of kinetic and magnetic energy (Fig. 4.12) shows, that the system reached the steady state of the velocity and temperature structure, with the magnetic field increasing (the difference between E_k and E_m is one order less than in the first simulation), but still in the "weak field dynamo" mode.

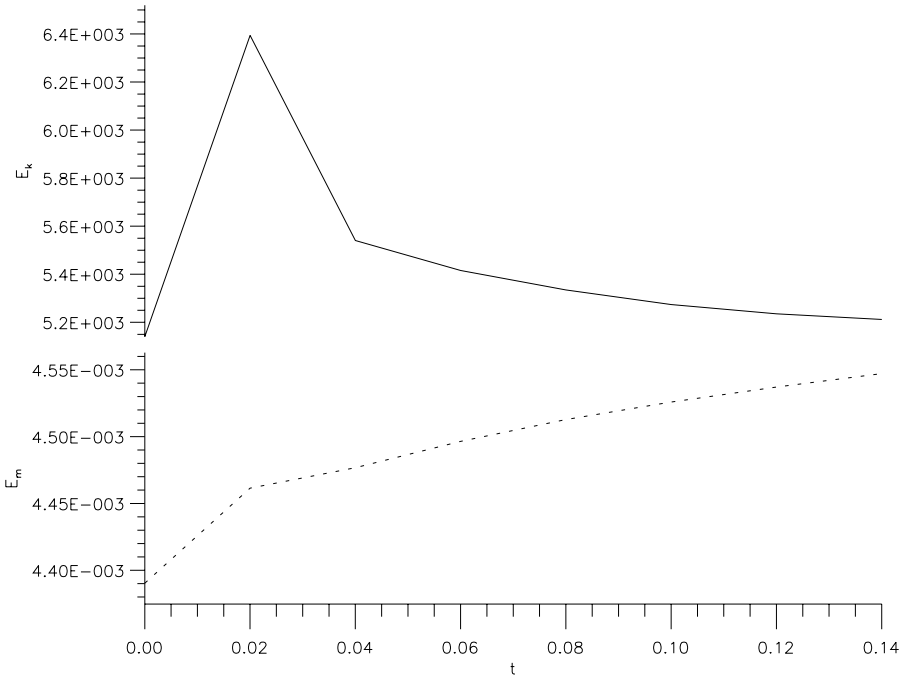

Figure 4.12: Case II. Time evolution of the kinetic energy of the fluid and the energy of the magnetic field.

4.5 Case III

The last model, that we have computed, includes the effects of viscous, adiabatic and Joule heating. We started the computation from the final state of Case I and evolved the system for $t = 0.13$.

The additional terms in the energy equation have considerably changed the pattern of the flow in the box. The temperature field (see Figs. 4.13, 4.14 and 4.15) almost linearly depends on the vertical coordinate z, with small horizontal perturbations. However, the fluid still circulates in the box with maximum velocities 2.4 in the horizontal direction and 16 in the vertical direction. The flow structure is more complicated, but still shows certain symmetry. The material flows upwards nearby the opposite sidewalls $y = 0$ and $y = a_y$ and descends to the bottom nearby the sidewalls $x = 0$ and $x = a_x$. The central area of the box is relatively calm.

The average Coriolis force (Fig. 4.16) is relatively weaker than in Case I (about 1% of the buoyancy force), because the ratio of the vertical motions to

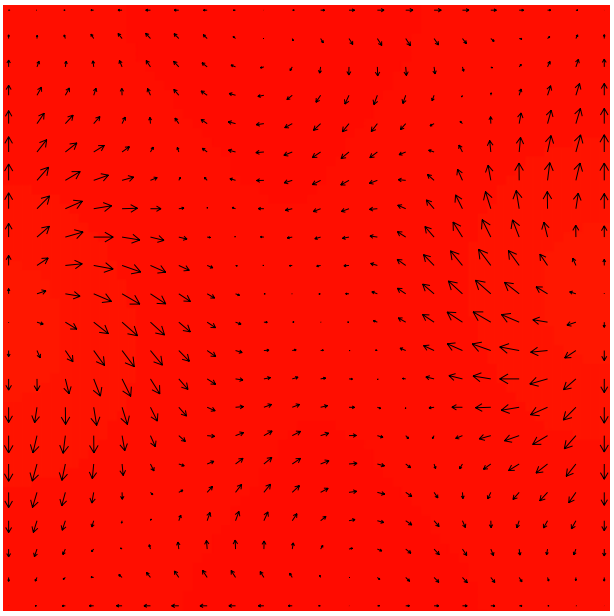

(a)

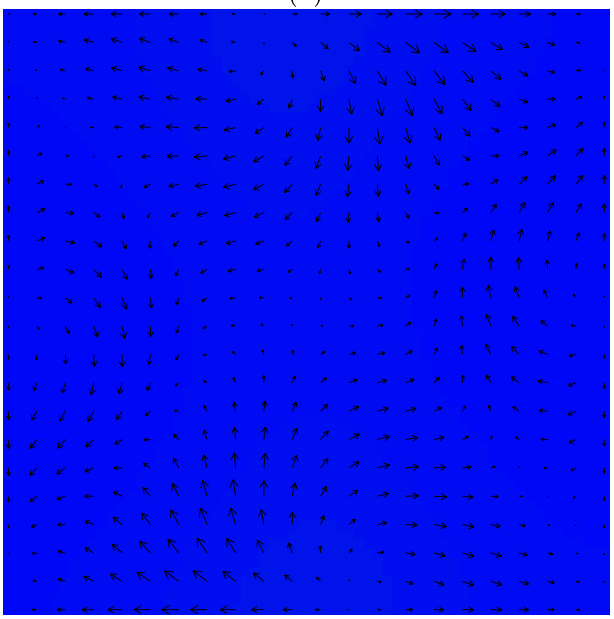

(b)

Figure 4.13: Case III. Temperature and projection of velocity in horizontal planes xy for (a) $m = 1$, (b) $m = 62$.

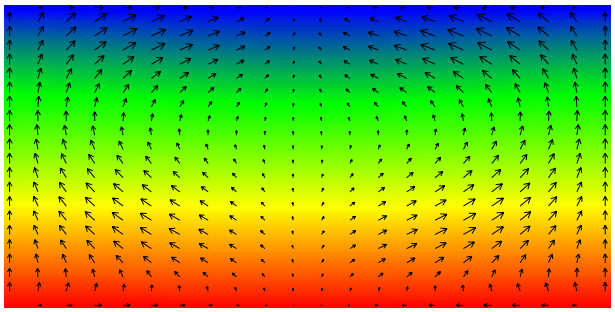

Figure 4.14: Case III. Temperature and projection of velocity in vertical plane yz for $k = 32$.

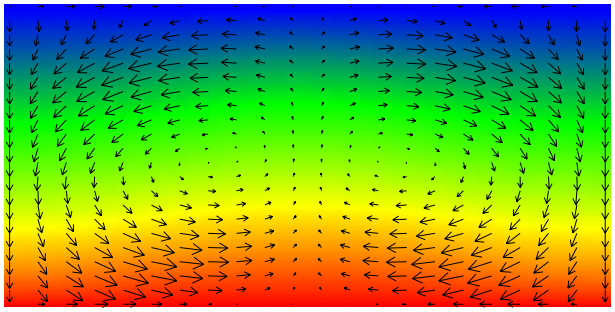

Figure 4.15: Case III. Temperature and projection of velocity in vertical plane xz for $l = 32$.

the horizontal motions is greater in Case III and only the later are significant in the term $\vec{k} \times \vec{v}$. Nevertheless, we can find the clockwise rotation of the horizontal velocity above the bottom and under the top of the box. The Lorentz force is negligible as it was in the previous cases.

At the beginning of this simulation, the viscous heating was about 40% of the adiabatic heating. As the fluid motion slowed in time, the importance of the viscous heating also decreased to 7% of the adiabatic term (see Fig. 4.17), which is responsible for the vertical stratification of temperature. The feedback from the magnetic field to the energy equation, the Joule

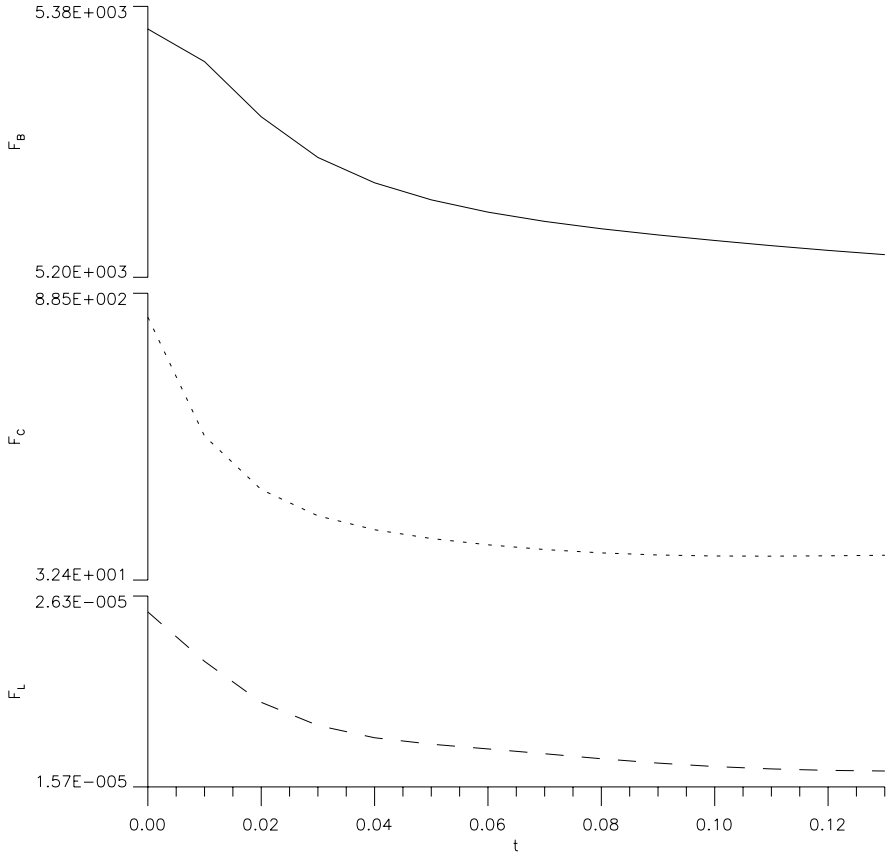

Figure 4.16: Case III. Time evolution of average buoyancy force F_B (solid line), the Coriolis force F_C (dotted line) and the Lorentz force F_L (dashed line).

heating, is again unimportant.

There are no significant differences in the magnetic field pattern from the previous cases (Figs. 4.18, 4.19). It was less then 0.0002 in the horizontal direction and up to 0.0014 in the z-axis direction.

The kinetic energy of the fluid decreased by one order during the evolution, due to the adiabatic and viscous heating (Fig. 4.20). Unlike in previous cases, the magnetic energy also decreased, though only by one third.

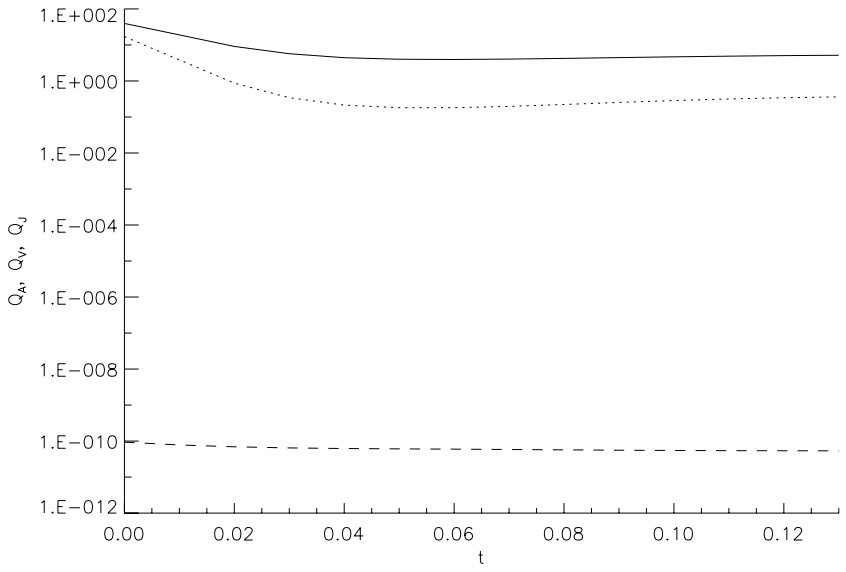

Figure 4.17: Case III. Time evolution of the average adiabatic heating Q_A (solid line), the average viscous heating Q_V (dotted line) and the average Joule heating Q_J (dashed line).

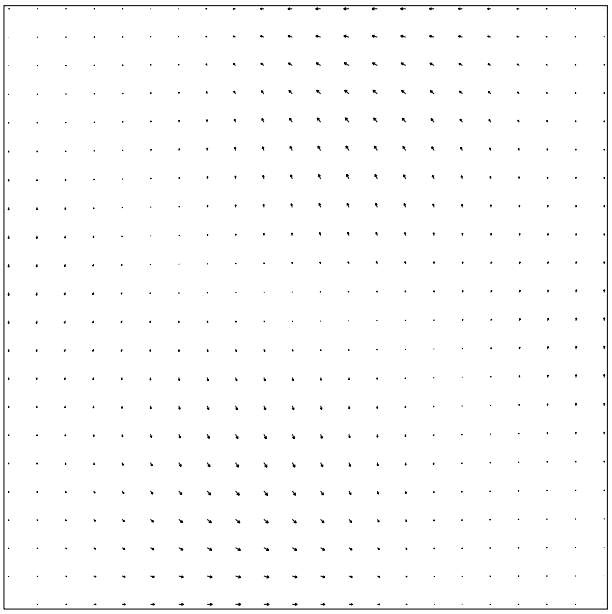

(a)

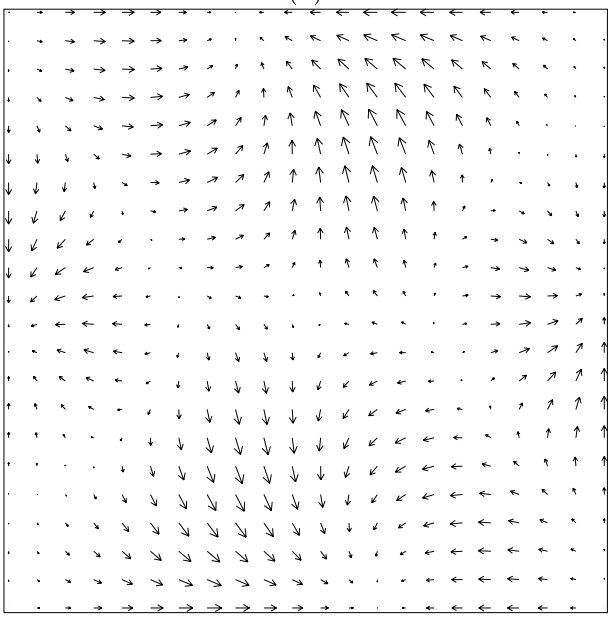

(b)

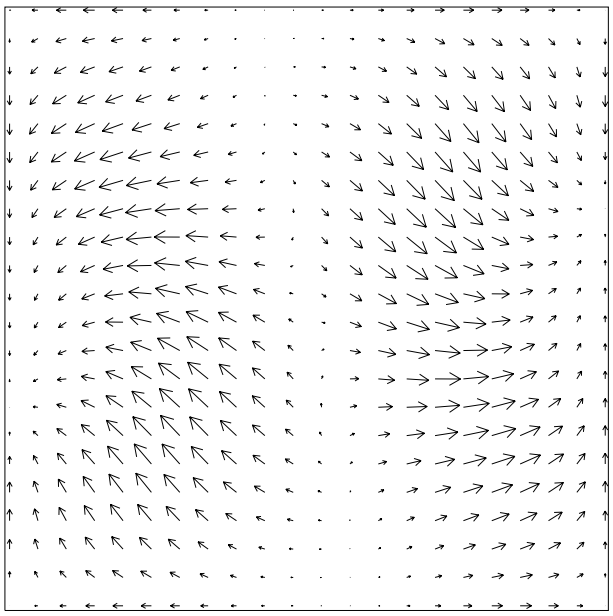

(c)

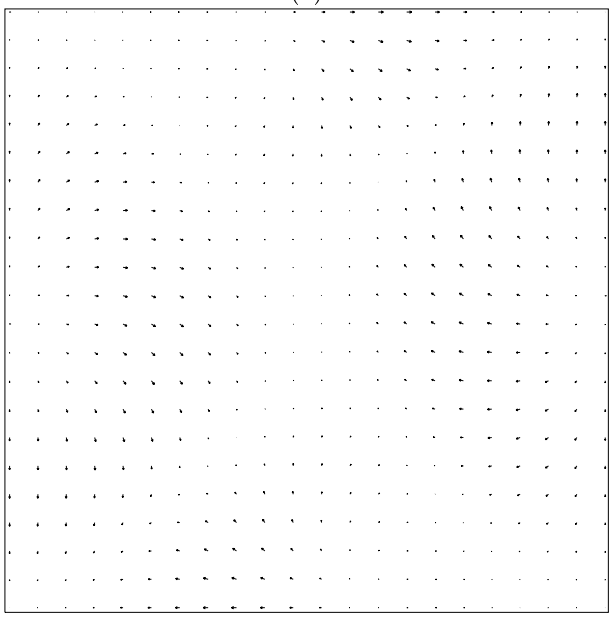

(d)

Figure 4.18: Case III. Projection of magnetic induction in horizontal planes xy for (a) $m = -20$, (b) $m = 1$, (c) $m = 32$, (d) $m = 62$.

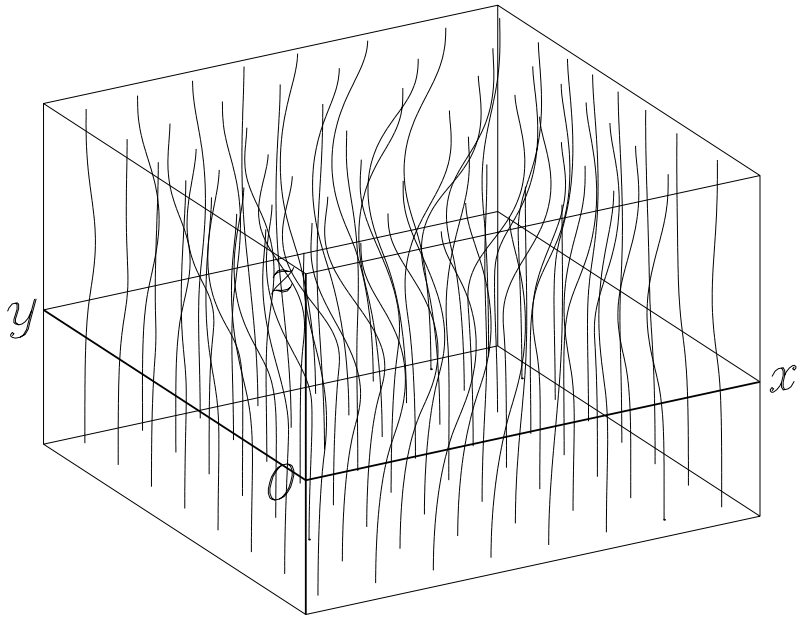

Figure 4.19: Case III. Magnetic induction.

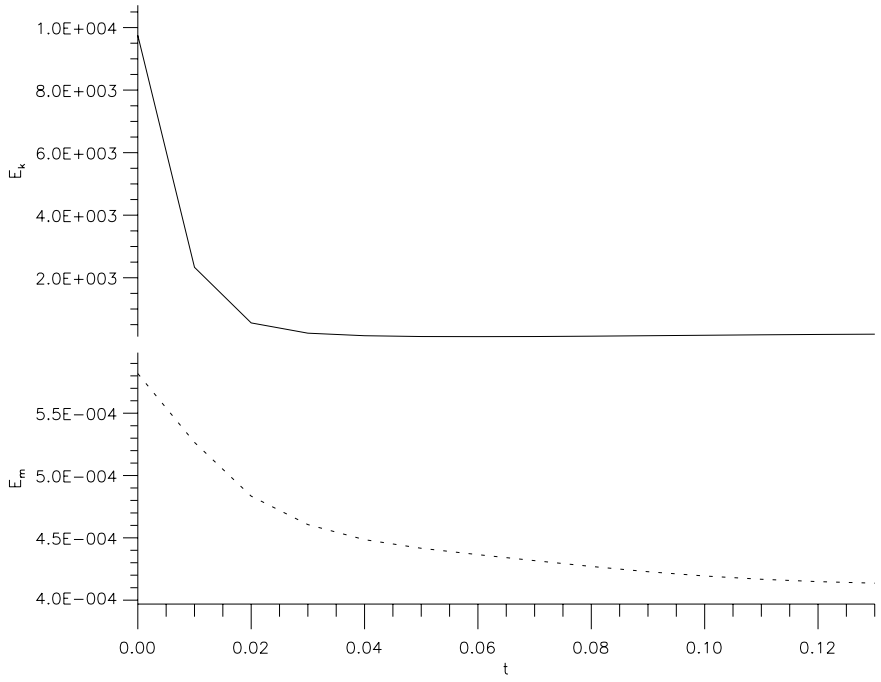

Figure 4.20: Case III. Time evolution of the kinetic energy of the fluid and the energy of the magnetic field.

4.6 Numerical Stability

In this section we will discuss the advantages and disadvantages of mathematical and numerical methods applied to the problem. First, we will concentrate on the fast Fourier transform, that we used to compute the velocity from the vorticity field. In [11] this problem was solved with an iterative Alternating Direction Implicit scheme and it was necessary to introduce another physical quantity — the vector potential. Unlike this, the Fourier transform can be computed "in place", with almost no additional memory needs and it is also faster. However, it has two disadvantages. Firstly, it limits the number of grid points to the integer power of two, which is more or less an inconvenience and secondly, it forces us to use the regular grid. This is more serious, because an irregular grid would allow us to increase the resolution in critical areas near the bottom and the top of the box without increasing the memory requirements. The lower resolution in boundary areas is the reason, why our attempts to simulate the chaotic flow

(with Rayleigh number greater than 10^4) or to use rigid boundary conditions $(\vec{v} = 0)_{ICB,CMB}$ have failed.

Another problem that deserves closer look is how to maintain the Maxwell equation (2.18) valid. We have showed in *Chapter 2*, that this equation can be considered as an initial condition for (2.67). However, the numerics always introduces some errors, so even the divergence of homogeneous vertical magnetic field (approximated by finite differences) at the start of Case I was non-zero (Fig. 4.21). The time dependence of the average divergence D_B shows similar history as the evolution of the magnetic energy (Figs. 4.6, 4.12 and 4.20), though the relative changes are smaller. There are two other ways, how to solve this problem (if we do not want to move to the spectral domain). We could use the evolution equation (2.67) to solve only two components of the magnetic induction and to compute the third one from the divergence-free condition (for example by using again the 3D Fourier transform) or we could separate the magnetic field in toroidal and poloidal components, which satisfy (2.18) automatically. However, this would increase the order of differentiation in the induction equation.

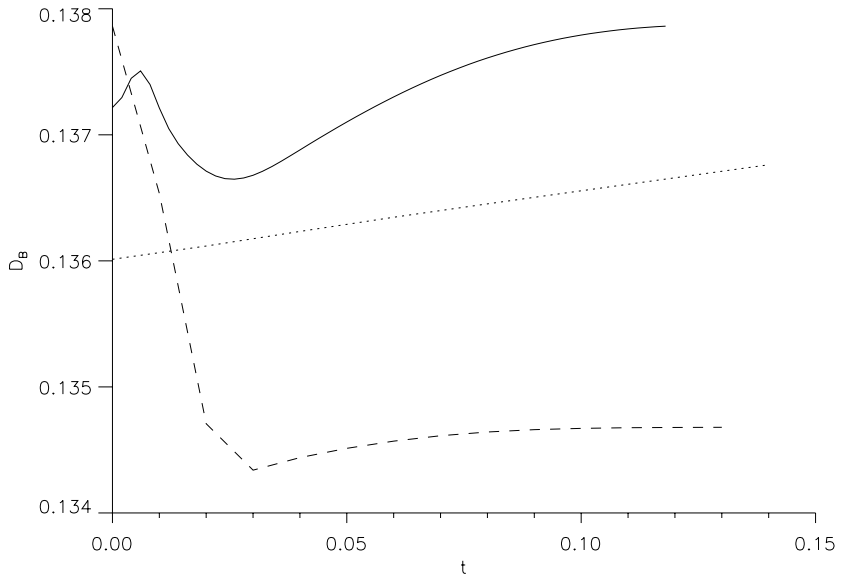

Figure 4.21: Time evolution of the average magnetic field divergence D_B for Case I (solid line), Case II (dotted line) and Case III (dashed line).

Chapter 5

Conclusions

We have simulated the behaviour of magnetohydrodynamic system with thermal driving in rectangular box for three sets of controlling parameters. The results, that we have achieved lead us to the following conclusions:

1. All simulations resulted in a steady state, highly symmetric flow and temperature patterns. The main reason of this behaviour is the choice of low Rayleigh number.

2. Increased Taylor number in Case II changed the pattern of the flow. The Coriolis force became almost as important as the buoyancy force.

3. The adiabatic heating (cooling) and the viscous dissipation in Case III decreased the lateral changes of temperature. The temperature field was close to the conductive profile with almost linear dependency on the z-coordinate. The velocity pattern also changed, the convection slowed down, but did not cease to work.

4. In all three cases so called "weak field dynamo" was evolved, with magnetic energy several orders below the kinetic energy of the fluid. The studied model can be called kinematic, because the feedback from the magnetic field to the convection (through the Lorentz force and Joule heating) was negligible.

5. The steady state convection with low Rayleigh and Taylor number was able to maintain, and in Cases I and II even to increase the magnetic field.

Although the system of equations, that we have solved is suitable for the Earth's outer core (with possible replacement of the Boussinesq approximation by the anelastic one), the choice of the computational domain and especially the choice of physical parameters of the fluid brought us very far from the problem of the geodynamo. The main differences between our model and the situation in the outer core are:

1. The rectangular shape of the domain in which we solved the magnetohydrodynamic equations introduces new boundary planes and leads to symmetries in the flow structure.

2. High Rayleigh and Taylor numbers in the core correspond to higher buoyancy driving as well as to increased effects of the Coriolis and Lorentz force. As a result, the material of the core flows faster and the system behaves chaotically.

3. The magnetic field of the core is several orders greater than in the simulation. Therefore, the Joule heating and the Lorentz force affect the flow and temperature patterns. In other words, the geodynamo is a "strong field dynamo". From this point of view, our simulation would correspond to the onset of the geodynamo, when the weak magnetic field in the interplanetary space served as an initial state.

Further improvements of the model are possible. Better spatial resolution, above all in the boundary layers is necessary to evolve the system with higher Rayleigh and Taylor numbers or with rigid boundaries. Decreasing the order of the equation of motion by abandoning the vorticity scheme could also improve the computation. It would be also possible to start the simulations with higher initial magnetic field, however better treatment of the divergence-free condition for the magnetic field could be necessary. All these changes would bring the model closer to the real problem, though evidently only the spherical models can simulate the generation of the Earth's magnetic field in its whole complexity.

References

[1] Anufriev A.P., Cupal I., Magnetic Field at the Core Boundary in the Nearly Symmetric Hydromagnetic Dynamo Z, Studia geophysica et geodetica, 31, 37–42, 1987.

[2] Braginsky S.I., Roberts P.H., Equations Governing Convection in Earth's Core and the Geodynamo, Geophys. Astrophys. Fluid Dynamics, 79, 1–97, 1995.

[3] Bucha V., Geomagnetické pole a jeho přínos k objasnění vývoje Země, Academia, Praha, 1975.

[4] Busse F.H., Theory of the Geodynamo and Core-Mantle Coupling, in: Chaotic Processes in the Geological Sciences, The IMA Volumes in Mathematics and its Applications, ed. Yuen D.A., Springer-Verlag, New York, 1992.

[5] Cardin P., Olson P., Chaotic Thermal Convection in a Rapidly Rotating Spherical Shell: Consequences for Flow in the Outer Core, Phys. Earth Planet. Inter., 82, 235–259, 1994.

[6] Fornberg B. A Practical Guide to Pseudospectral Methods, Cambridge Univ. Press, Cambridge, 1996.

[7] Glatzmaier G.A., Roberts P.H., A Three-Dimensional Convective Dynamo Solution with Rotating and Finitely Conducting Inner Core and Mantle, Phys. Earth Planet. Inter., 91, 63–75, 1995.

[8] Glatzmaier G.A., Roberts P.H., An Anelastic Evolutionary Geodynamo Simulation Driven by Compositional and Thermal Convection, preprint, 1997.

[9] Lavičková R., Spectral Characteristic of MHD Equations, dipl. thesis in preparation, Faculty of Mathematics and Physics, Charles University, Praha, 1998.

[10] Malevsky A.V., Spline-Characteristic Method for Simulation of Convective Turbulence, Journal of Computational Physics, 123, 466–475, 1996.

[11] Mistr Z., Fluid Dynamics in the Earth's Outer Core, Effects of Rotation and Adiabatic Heating, dipl. thesis, Faculty of Mathematics and Physics, Charles University, Praha, 1996.

[12] Press W.H., Teukolsky S.A., Vetterling W.T. and Flannery B.P., Numerical Recipes in Fortran, Second Edition, Cambridge Univ. Press, Cambridge, 1992.

[13] Roberts P.H., Dynamo Theory, in: Chaotic Processes in the Geological Sciences, The IMA Volumes in Mathematics and its Applications, ed. Yuen D.A., Springer-Verlag, New York, 1992.

[14] Secco R.A., Viscosity of the Outer Core, in: Mineral Physics & Crystallography, AGU, 1995.

[15] Vitásek E., Numerické metody, SNTL, Praha, 1987.

Acknowledgements

Tato diplomová práce byla podporována z grantu UK č. 170/1998 *Počítačové simulace nelineární planetární dynamiky.*

V prvé řadě děkuji svému vedoucímu, doc. RNDr. Ctiradu Matyskovi, DrSc., za četné rady a připomínky, bez kterých by tato práce nevznikla. Jeho bohaté zkušenosti mi byly velkou oporou a jeho optimismus mi dodával chuť do další práce.

Doc. RNDr. Jiřímu Zahradníkovi, CSc. vděčím za vytvoření takových podmínek k práci, o jakých se mi ani nesnilo. RNDr. Ladislavu Hanykovi děkuji za pomoc ve věčném zápase s počítači, ve kterém nemůžeme zvítězit a našim seismologům za strojový čas a diskový prostor, který mi poskytli. Všem členům katedry geofyziky, jejím doktorandům i studentům pak děkuji za přátelské ovzduší, které zde panuje.

RNDr. Ivanu Cupalovi, CSc. z Geofyzikálního ústavu AV ČR dlužím dík za možnost zúčastnit se semináře v Třešti i za konzultaci, kterou mi tam poskytl.

Tuto práci věnuji svým rodičům. Budiž jim malou odměnou za jejich velkou podporu, starostlivost a lásku.